

Universal stability of coherently diffusive 1D systems with respect to decoherence.

F. S. Lozano-Negro,¹ E. Alvarez Navarro,² N. C. Chávez,³ F. Mattiotti,⁴ F. Borgonovi,^{3,5} H. M. Pastawski,¹ and G. L. Celardo⁶

¹*Instituto de Física Enrique Gaviola (CONICET-UNC) and Facultad de Matemática, Astronomía, Física y Computación, Universidad Nacional de Córdoba, 5000, Córdoba, Argentina*

²*Benemérita Universidad Autónoma de Puebla, Apartado Postal J-48, Instituto de Física, 72570, Mexico*

³*Dipartimento di Matematica e Fisica and Interdisciplinary Laboratories for Advanced Materials Physics, Università Cattolica, via della Garzetta 48, 25133 Brescia, Italy*

⁴*University of Strasbourg and CNRS, CESQ and ISIS (UMR 7006), aQCess, 67000 Strasbourg, France*

⁵*Istituto Nazionale di Fisica Nucleare, Sezione di Milano, via Celoria 16, I-20133, Milano, Italy*

⁶*Department of Physics and Astronomy, CSDC and INFN, Florence Section, University of Florence, Italy*

Static disorder in a 3D crystal degrades the ideal ballistic dynamics until it produces a localized regime. This Metal-Insulator Transition is often preceded by coherent diffusion. By studying three different paradigmatic 1D models, the Harper-Hofstadter-Aubry-André and the Fibonacci tight-binding chains, and the power-banded random matrix model, we show that whenever coherent diffusion is present, transport is exceptionally stable against decoherent noise. This is completely at odds with what happens for ballistic and localized dynamics, where the diffusion coefficient strongly depends on the environmental decoherence. A universal dependence of the diffusion coefficient on the decoherence strength is analytically derived: the diffusion coefficient remains almost decoherence-independent until the coherence time becomes comparable with the mean elastic scattering time. Thus, systems with a quantum diffusive regime could be used to design stable quantum wires and may explain the functionality of many biological systems, which often operate at the border between the ballistic and localized regimes.

Introduction. The control of quantum transport in presence of environmental noise is crucial in many areas: cold atoms [1–4], mesoscopic systems [5–7], and quantum biology [8–11]. Thus, its better understanding would allow us to build more precise quantum channels of communication [12], to design more efficient sunlight harvesting systems [10, 11, 13–17], devices that transfer charge or energy with minimal dissipation [18, 19], and bio-mimetic photon sensors [20], as well as to understand the functionality of many biological aggregates [21–27].

P. W. Anderson [28, 29], realized that elastic scattering from random disorder exceeding a critical value induces the localization of quantum excitations, i.e. the *metal-insulator transition* (MIT) [30]. While in 3D this critical disorder is finite, in 1D it is negligible. It took over two decades to realize that correlated disorder and long-range hopping could allow a MIT even in 1D [31–34]. R. Landauer [35], N. Mott [36, 37], and H. Haken [38] considered the different roles of the environment. Landauer noticed that an actual finite system exchanges particles with external reservoirs through the current and voltage probes, a notion that M. Büttiker used to describe environmental decoherence and thermalization [39–41]. Both, Haken and Mott sought to address the role of a thermal bath. The Haken-Strobl model describes uncorrelated dynamical fluctuations in the site energies, which is equivalent to an infinite temperature bath. Later on, Mott predicted a *variable-range-hopping* regime in which energy exchange among phonons and Anderson’s localized states would favor conductivity before decoherence freezes the dynamics [42]. Thus, in the localized regime, the 1D conductivity reaches a maximum [15, 40, 43–46] when the energy uncertainty associated with elastic scattering and

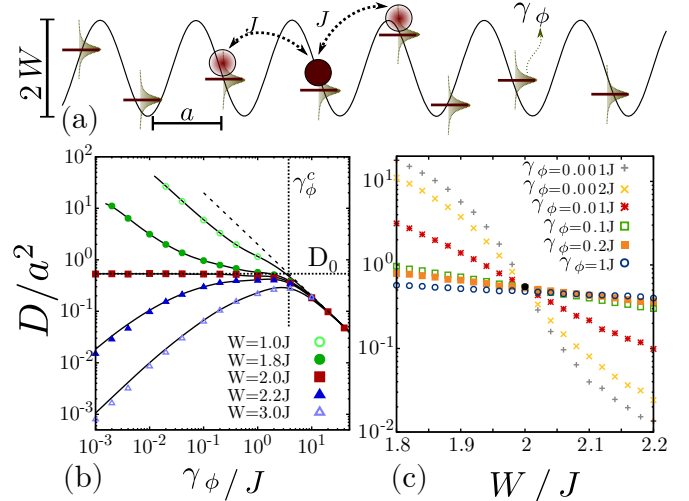


FIG. 1. (a) HHAA chain: horizontal lines are local energies, Lorentzian uncertainties indicate decoherence. (b) Scaled diffusion coefficient D/a^2 vs. the decoherence $\gamma\phi/J$ for different W 's. Solid black curves result from Eq. (6). Different regimes are extended (green), critical (red), and localized (blue). The black dotted line is the coherent theoretical estimate D_0/a^2 ; the black dashed line is the asymptotic $D/a^2 \simeq 2J^2/\hbar\gamma\phi$ and the vertical dot-dashed line is the characteristic decoherence $\gamma\phi_c/J$. (c): Diffusion coefficient D/a^2 vs. the W/J for different $\gamma\phi$'s. Numerical data obtained by the QD method for $N = 1000$, $q = (\sqrt{5} - 1)/2$, $J = 1$ and $\hbar = 1$.

that resulting from the coupling with the environment (i.e. decoherence processes) [47–50] are comparable. In contrast, the ballistic dynamic of a perfect crystal is always degraded by decoherent scattering processes, induc-

ing diffusion. *However, a much less studied subject is how decoherent noise affects transport at the MIT and, more generally, in presence of a quantum diffusive-like dynamics.*

Recent works on excitonic transport in large biomolecules such as photosynthetic antenna complexes seek to explain the puzzling great efficiency of many natural [15, 44, 51–54] and synthetic systems. In this context, S. Kauffman [55] proposed the intriguing *poised realm* hypothesis that, in biological systems, excitation transport occurs at the *edge of chaos* [56]. This led Vattay and coll. [57] to propose that 1D systems near the MIT are optimal for transport because environmental decoherence does not affect the system as strongly as it does in the extended regime while it provides enough delocalization to allow good transport.

This seems at odds with an early theoretical analysis [41] indicating that it is the intrinsic diffusive dynamic of some 1D systems that yields stability towards decoherence. This resembles what occurs with the residual resistivity of impure 3D metals at low temperatures. With the purpose to settle this conflict, we study paradigmatic coherently-diffusive models. We first analyze the Harper-Hofstadter-Aubry-André (HHAA) model [31], see Fig. 1a, which has been brought to the spotlight [58–61] thanks to its recent experimental implementations [62–65]. We found, both numerically and analytically, that only at the MIT the second moment of an initially localized excitation can be described by a diffusion coefficient D . Below a characteristic decoherence strength γ_ϕ^c , see Fig. 1b, D is very weakly dependent on the decoherent noise. We also show that, at long times, D determines the current and the *Loschmidt echo* (LE) decay. Thus, at the MIT, both magnitudes are almost independent of the noise strength. However, these findings do not settle the question of whether it is the diffusive quantum dynamic what brings stability towards decoherence or if this stability is inherent to the critical point. For this reason we also studied the Fibonacci chain [66] and the *power-banded random matrices* (PBRM) [34], where a diffusive-like regime exists in some parameter range independently of their critical features. Our results show that, whenever a system is in a quantum coherent diffusive regime, transport is extremely stable towards decoherence, even outside the critical point. Moreover, all models follow a universal expression for D , depending only on a single parameter: the ratio between the elastic scattering and the decoherence time.

The letter is organized as follows: we first focus on the HHAA model, explaining the methods and the results. We then introduce our analytical quantum collapse picture which explains and extends these results. A further analysis of the Fibonacci and the PBRM models demonstrate the universality of our results.

Model and Methods: HHAA, Haken-Strobl and quantum-drift. The HHAA model [31, 67, 68], Fig. 1a, describes a linear chain with hopping amplitude J among sites $|n\rangle$ at distance a modulated by a local potential ε_n ,

according to the Hamiltonian:

$$\mathcal{H} = \sum_n -J(|n\rangle\langle n+1| + |n+1\rangle\langle n|) + \varepsilon_n |n\rangle\langle n|, \quad (1)$$

where $\varepsilon_n = W \cos(2\pi qna + \theta)$, $q = q_g = (\sqrt{5} - 1)/2a$ and $0 < \theta < 2\pi$ is a random phase over which we average in numerical simulations. Other values of q are discussed in the SM [69] Sec. V. Contrary to the Anderson 1D model, the HHAA model presents a phase transition as the eigenstates are extended for $0 \leq W < 2J$ and localized for $W > 2J$ [31, 67]. A notable trait is that the MIT occurs exactly for $W = 2J$ in the whole spectrum and that all eigenstates have the same localization length $2\xi = a/\ln[W/2J]$ [31, 70] for $W > 2J$.

The presence of a local white-noise potential is described by the Haken-Strobl (HS) model [71, 72], widely used for excitonic transport. The environment is described by stochastic and uncorrelated fluctuations of the site energies $V(t) = \sum_n \varepsilon_n(t) |n\rangle\langle n|$, with $\langle \varepsilon_i(t) \rangle = 0$ and $\langle \varepsilon_n(t) \varepsilon_m(t') \rangle = \hbar \gamma_\phi \delta_{nm} \delta(t - t')$. The dynamics can be described by the Lindblad master equation:

$$\dot{\rho} = \mathcal{L}[\rho] = -\frac{i}{\hbar} [\mathcal{H}\rho - \rho\mathcal{H}] + \mathcal{L}_\phi[\rho], \quad (2)$$

with:

$$\mathcal{L}_\phi[\rho] = \frac{\gamma_\phi}{\hbar} \sum_{n=1}^N \left[|n\rangle\langle n| \rho |n\rangle\langle n| - \frac{1}{2} |n\rangle\langle n| \rho - \frac{1}{2} \rho |n\rangle\langle n| \right], \quad (3)$$

where γ_ϕ/\hbar is the dephasing rate. It induces a diffusive spreading of the excitation in the infinite size limit of tight-binding models [47, 73]. The HS master equation leads to a stationary equally probable population on all sites, corresponding to an infinite temperature bath [13, 74, 75] and it is a good approximation when the thermal energy is of the same order of the spectral width of the system (as it happens in many biological systems [15, 76, 77]).

Solving the master equation requires to handle $N^2 \times N^2$ matrices. To overcome this limit we use the *quantum-drift* (QD) model [75], an approach conceived as a realization of the Büttiker's local voltage probes [41] in a dynamical context [78, 79]. Here, the system wave function follows a Trotter-Suzuki dynamics. Local collapse processes are represented as local energies fluctuating according to a Poisson process [75, 79]. This yields local energies with a Lorentzian distribution of width $\gamma_\phi/2$ (for details see SM [69] Sec. II), allowing us to handle more than 10^4 sites.

The diffusion coefficient $D = \sigma^2(t)/(2t)$ is computed numerically through the variance $\sigma^2(t) = a^2 [\sum_n \rho_{n,n}(t) n^2 - (\sum_n \rho_{n,n}(t) n)^2]$ starting from a local initial excitation in the middle of the chain. Our results have been confirmed using the Green-Kubo approach [47], see SM [69] Sec. IV A.

Coherent dynamics in HHAA. In absence of dephasing the short and long time behavior of the variance $\sigma_0^2(t)$

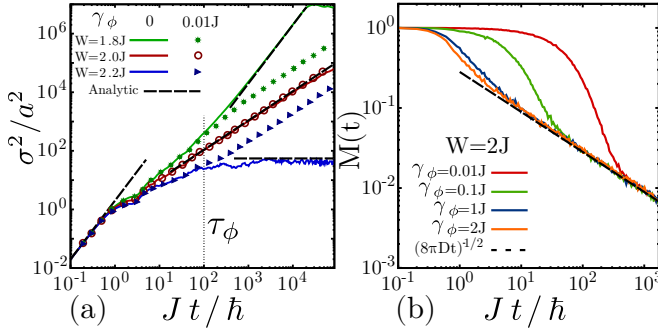


FIG. 2. (a) Excitation spreading for the HHAA model with $N = 10000$ for different W . Coherent dynamics are the solid curves while symbols show decoherent ones, $\gamma_\phi = 0.01J$. Black dashed lines are the analytical estimates for $\gamma_\phi = 0$, see text. The vertical dotted line shows the decoherence time $\tau_\phi = \hbar/\gamma_\phi$. (b) Loschmidt echo decay $M(t)$ for different γ_ϕ at the critical point $W = 2J$ and $N = 1000$. The solid lines result from the QD. The dashed line is the theoretical predictions based on a coherent diffusion. All data have $q = (\sqrt{5} - 1)/2$, $J = 1$, $\hbar = 1$.

can be computed analytically, see SM [69] Sec. III. In all regimes, the initial spreading is always ballistic, $\sigma_0^2(t) = v_0^2 t^2$, with a velocity $v_0^2 = 2a^2(J/\hbar)^2$. After this transient regime, we have: i) for $W < 2J$ and large times, the spreading is still ballistic, but with a different *mean group velocity*: $u^2 = a^2|2J - W|^2/2\hbar^2$, see solid green curve in Fig. 2a; ii) for $W > 2J$, localization occurs [80, 81] and we have $\sigma_0^2(\infty) = 2\xi^2 = 2a^2(2\ln(W/2J))^{-2}$, see solid blue curve in Fig. 2a and iii) at the MIT for $W = 2J$, the variance grows diffusely, $\sigma_0^2(t) = 2D_0 t$, see Fig. 2a. This is consistent with Ref. [82], where deviations from a diffusive regime are shown not to affect the variance at criticality up to extremely large system sizes ($N \approx 10^{10}$), after which a weak super-diffusive dynamics will emerge.

The diffusion coefficient $D_0 = (v_0^2 \tau_W)/2$ at the MIT depends on both the initial velocity v_0 and the *mean elastic scattering time* τ_W over which local inhomogeneities manifest themselves in the dynamics of a *local* excitation [83]:

$$\tau_W = \hbar/\Delta E, \quad \text{where} \quad (\Delta E)^2 = \langle (\mathcal{H}_{n,n} - \mathcal{H}_{n+1,n+1})^2 \rangle / 2 \quad (4)$$

where $\mathcal{H}_{n,n} = \langle n | \mathcal{H} | n \rangle$ and $\langle \dots \rangle$ represents the average over all Hamiltonian diagonal elements. When considering disordered models, $\langle \dots \rangle$ also includes average over disorder. For the HHAA model we have $(\Delta E)^2 = W^2(1 - \cos(2\pi q))/2$, see SM [69] Sec. III B, so that:

$$D_0 = \frac{a^2}{\hbar} \frac{J^2}{W \sqrt{[1 - \cos(2\pi q)]/2}}. \quad (5)$$

which we checked to be in very good agreement with the numerical results at the MIT, see Fig. 2a and SM [69] Sec. V.

Decoherence in the HHAA model. When the system is in contact with an environment, the time-dependent

fluctuations of the site energies affect the dynamics, inducing a diffusive behavior. In Fig. 2a we show (symbols), for $W < 2J$ and $W > 2J$, how the dynamics becomes diffusive after $\tau_\phi \approx \hbar/\gamma_\phi$ (see vertical dotted line). In general, the diffusion coefficient depends on the decoherence strength, apart at the MIT, where, interestingly, the dynamic remains diffusive with a diffusion coefficient very close to D_0 as in absence of noise, see also Fig. 1b,c.

In Fig. 1b we show that in the extended regime, D decreases with the decoherent strength, while in the localized regime D reaches a maximum. Remarkably, at the MIT, D is almost independent from decoherence up to γ_ϕ^c defined as $\gamma_\phi^c = 2\hbar/\tau_W$, see vertical line in Fig. 1b. Fig. 1c shows D vs. the on-site potential strength for different decoherence strengths. As one can see all curves intersect at $W = 2J$, suggesting the independence of decoherence precisely at the MIT.

The quantum collapse picture. In order to understand the exact dependence of D on γ_ϕ we apply a quantum collapse model for the environmental noise. The latter can be assimilated to a sequence of measurements of the excitation's position [75, 84, 85], inducing local collapse that leads to a random walk [41, 45, 77, 86]. Then D can be readily determined from $\sigma_0^2(t)$ as:

$$D \simeq \frac{\int_0^\infty dt_i p(t_i) \sigma_0^2(t_i)}{2\tau}, \quad (6)$$

where $p(t_i)$ is the probability density of measurement at time t_i and $\tau = \int_0^\infty dt_i t_i p(t_i)$, details are given in SM [69] Sec. IV B. Since the HS model corresponds to a Poisson process for the measurement collapses [75], $p(t_i) = e^{-t_i/\tau_\phi}/\tau_\phi$. Using Eq. (6) we obtain results in excellent agreement with numerical data, see black curves in Fig. 1b. The independence of D from γ_ϕ can be derived from Eq. (6) only by assuming a diffusive dynamics in absence of dephasing $\sigma_0^2(t) = 2D_0 t$, see SM [69] Sec. IV B.

Loschmidt echo/purity decay in the HHAA model. The robustness of the wave packet spreading at the MIT, naturally leads to the question of how current and coherences are affected by decoherence. We found that the steady state current is fully determined by the diffusion coefficient, thus showing the same robustness to decoherence at the MIT, see SM [69] Sec. I. The rate at which the environment destroys coherences has been studied through the decay of the Loschmidt echo or purity [87–89], $M(t) = \text{Tr}[\rho(t)^2]$ that can be computed efficiently using the Quantum Drift method, see SM [69] Sec. VII. As we start from a pure state, $M(0) = 1$, and reaches $M(t) \rightarrow 1/N$ when $\rho(t)$ becomes a full mixture of N equally probable states. We find that, for all values of W/J , the long-time decay of the purity is a power law determined only by the diffusion coefficient: $M(t) \sim \sqrt{8\pi D t}$, which at the MIT is extremely robust to decoherence, see Fig. 2b.

All the above results could be experimentally tested in Yb cold atoms in a 1D optical lattice where the HHAA model was already implemented [63, 90, 91]. Local deco-

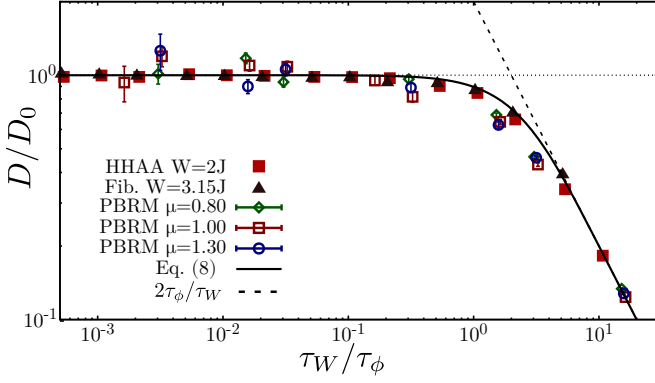


FIG. 3. Normalized diffusion coefficient D/D_0 vs. decoherence τ_W/τ_ϕ ($D_0 = D(\gamma_\phi = 0)$). Symbols obtained from QD dynamics: **i)** the HHAA chain at criticality (red squares), **ii)** the Fibonacci chain (dark-red triangles) and **iii)** the PBRM model in the extended phase (green hollow-diamond), at the critical point (red hollow-squares) and in the localized phase (blue hollow-circles). The solid curve is the universal Eq. (8) while the dashed-black line is the limit of $\tau_W/\tau_\phi > 2$. Horizontal dotted line is $D = D_0$. For the HHAA and the Fibonacci chains, τ_W and D_0 were computed analytically, Eq. (4). For the PBRM model, D_0 results from a fitted τ_W .

herence could be imposed [92] by time-dependent white noise fluctuations that exploit speckle patterns uncorrelated in time and space.

Analysis of the Fibonacci and PBRM models. In order to understand whether the robustness found in the HHAA model at criticality is due to the presence of a critical point or to the presence of a diffusive dynamics, we also studied other two models: A) the Fibonacci chain [66, 80, 93] where there is no MIT but transport changes smoothly from super-diffusive to sub-diffusive as the strength of the on-site potential is varied; B) The PBRM model [34] which presents a MIT and a diffusive second moment in a finite range of parameters around the MIT (see SM [69] Sec. VI). Since this model incorporates topologically different Feynman pathways it is often considered a 1^+D system.

The Fibonacci model [93] is described by the Hamiltonian (1), with on-site energies alternating among two values as in binary alloy models: $\varepsilon_n = W([\!(n+1)q_g^2\!] - [nq_g^2])$, where $[\dots]$ is the integer part. This model has no phase transition and the variance of an initial localized excitation grows in time as $\sigma_0^2(t) \propto t^\alpha$ where $0 < \alpha < 2$ depends continuously on the on-site potential strength [49, 94]. On the other side, the Hamiltonian matrix elements for the PBRM model are taken from a normal distribution with zero mean, and variance:

$$\langle |\mathcal{H}_{ij}|^2 \rangle = 1/(2 + 2(|i-j|/b)^{2\mu}) \text{ if } i \neq j, \quad (7)$$

and $\langle |\mathcal{H}_{ii}|^2 \rangle = 1$ for on-site energies. The model has a critical interaction range ($\mu = 1$), characterized by

a multi-fractal nature [95–97], for all values of b where the system switches from extended ($\mu < 1$) to localized ($\mu > 1$) eigenstates [34]. In this model, we have found a diffusive excitation spreading in absence of decoherence, not only at the critical point but in a much broader range of μ values $1/2 < \mu < 3/2$. Note that even for $1 \leq \mu \leq 3/2$, the saturation value of the variance grows with the system size, thus allowing a diffusive-like spreading in the infinite size limit, see SM [69] Sec. VI. This sounds counter-intuitive since for $1 \leq \mu \leq 3/2$ we are in the localized regime if the participation ratio of the eigenstates is used as a figure of merit for localization [34]. This peculiarity is due to the long-range hopping present in this model.

Universal stability towards decoherence. As we discussed below Eq. (6), if the coherent dynamics is diffusive at all times, then $D = D_0$ for all decoherence strengths. On the other hand, in the more realist case, where an initial ballistic dynamics, $\sigma_0^2(t) = v_0^2 t^2$ for $t < \tau_W$, is followed by a diffusive spreading $\sigma_0^2(t) = 2D_0 t$, Eq. (6) yields (see details in SM [69] Sec. IV B):

$$D(x)/D_0 = [2/x - (1 + 2/x)e^{-x}], \quad (8)$$

where $x = \tau_W/\tau_\phi$. This expression captures the dependence of D with large and small values of τ_W/τ_ϕ . For $\tau_W/\tau_\phi \ll 1$, the diffusion coefficient $D \approx D_0(1 - \frac{1}{6}(\frac{\tau_W}{\tau_\phi})^2)$. While for $\tau_W/\tau_\phi \gg 1$, we enter the strong quantum Zeno regime and $D/D_0 \approx 2\tau_\phi/\tau_W$.

Eq. (8) depends only on the ratio between the mean elastic scattering time and the decoherence time, thus it describes universally any 1D quantum mechanical model characterized by a coherent diffusive dynamics, independently of the details of their microscopic dynamics. Figure 3 shows the normalized diffusion coefficient D/D_0 in the three models (HHAA, Fibonacci, and PBRM). Analysis has focused only on the diffusive-like coherent dynamics regime for all models, where D_0 is well defined. The universal behavior predicted by Eq. (8) is in excellent agreement with the numerical results for all models.

The fact that a coherent diffusive quantum dynamics is extremely robust to the environmental noise is in striking contrast with what one would expect considering scattering (with a time scale τ_W) and environmental noise (with a time scale τ_ϕ) as two independent Poisson's processes. In this case, the two processes can be thought of as a single Poisson's process with a time scale $1/\tau = 1/\tau_W + 1/\tau_\phi$. Thus, for small values of $\tau_W/\tau_\phi \ll 1$, we have $D \approx D_0(1 - \tau_W/\tau_\phi)$, in contrast with the quadratic correction present in Eq. (8). Our findings are also in contrast with standard results in classical systems where the diffusion coefficient for the dynamics in presence of external noise is the sum of the diffusion coefficients given by the two processes [98].

Conclusions. By studying quantum transport in three paradigmatic 1D models, all of them with a quantum diffusive-like regime, we found a striking stability of transport towards decoherence which also shows up

in the Loschmidt echo/purity decay. This stability originates in the diffusive nature of the coherent quantum dynamics and it holds as long as the decoherence time is longer than the mean elastic scattering time. Moreover, in the coherent diffusive regime, we analytically derived a universal law in which the diffusion coefficient depends on a single parameter: the ratio between these characteristic times. We stress that this stability does not show up when a sample is in a ballistic or in a localized regime, where the diffusion coefficient is highly sensitive to decoherence. Nevertheless, as occurs in the PBRM model, in many quasi-1D systems the elastic mean-free-path may become much larger than the localization length [5, 99] and thus, the diffusion-like regime would occur in a wide range of parameters. Therefore, even when coherent diffusion only occurs in a limited length scale, it could be enough to ensure an efficient and stable transport under environmental noise in many realistic systems. Some actual conducting polymer composites, arranged in bundles with degenerate active channels, may be in the stability regime discussed here [100–104].

Apart from the cold atomic set-up where our findings could be verified as explained above, another situation that fits the above condition is nuclear spin diffusion in quasi 1D crystals [105, 106]. There, the natural dipolar interactions are long range and the disorder can be turned on and off through appropriate radio-frequency pulses. The NMR observation of spin excitations in this system shows both a ballistic and a quantum diffusive regimes. Notably, the spin-spin Ising many-body terms manifest as a decoherence timescale in an otherwise coherent propagation [60, 86, 106–108]. Further modification of these experiments [105, 106] could test the stability of the spin diffusion towards decoherence.

We foresee that our prediction may have a strong impact in the study of several quasi-1D biological systems, where robust charge or excitonic transport are functionally relevant. Among these are the helical DNA structures [109], where it seems crucial for energy transfer and its self-repair [110–113]. There, one might hint a role in the puzzling mechanism through which DNA transmits allosteric signals over long distances to boost the binding cooperativity of transcription factors [114]. In photosynthetic systems it is essential an efficient energy transport from the antenna complex to the reaction center followed

by a temperature independent electron transfer from a chlorophyll to a distant quinone [115]. This elicited the long standing question of whether transport of charges occurs as a coherent process through conduction bands, or through multiple decoherent tunneling hops between localized states [83, 116, 117]. Our decoherent diffusion hints at an alternative that deserves further study. In the antenna complex itself, there is a convergence of energy scales [77] (i.e. the couplings, disorder, and thermal fluctuations, are roughly of the same order), that could ensure the universally robust regime we discussed. Moreover, the analysis of the spectral statistics of several biologically relevant molecules suggest that they are typically at the border between a ballistic and a localized regime [8]. Indeed, some proteins, micro-tubules and RNA [21–27, 118–120], show a surprisingly robust transport against temperature induced decoherence [74, 121–124].

Our results give a new light to the hypothesis, promoted for biological systems, [55, 57], that being at the edge of chaos is favorable to charge or excitonic transport. Indeed, classical chaos is a road to diffusive dynamics [125, 126] and, as shown here, quantum diffusion-like dynamics is extremely robust with respect to environmental noise. In perspective, it would be interesting to analyze further signatures of intrinsic quantum diffusion in realistic biological systems in order to establish the functional relevance of our findings. We conjecture that quantum diffusion is a most relevant feature of Nature’s *poised realm*.

ACKNOWLEDGMENTS

FB and GLC thank L. Fallani and J. Parravicini for suggestion of the experimental realization of decoherence in cold atomic lattices. HMP thanks D. Chialvo for introducing S. Kauffman to him. GLC thanks E. Sadurni and A. Méndez-Bermúdez for useful discussions. The work of FSLN and HMP was possible by the support of CONICET, SeCyT-UNC and FonCyT. FB and GLC acknowledge support by the Iniziativa Specifica INFN-DynSysMath. This work has been financially supported by the Catholic University of Sacred Heart and by MIUR within the Project No. PRIN 20172H2SC4.

-
- [1] E. Akkermans, A. Gero, and R. Kaiser, *Phys. Rev. Lett.* **101**, 103602 (2008).
 - [2] E. Akkermans and A. Gero, *EPL* **101**, 54003 (2013).
 - [3] T. Bienaimé, N. Piovella, and R. Kaiser, *Phys. Rev. Lett.* **108**, 123602 (2012).
 - [4] R. Kaiser, *J. Mod. Opt.* **56**, 2082 (2009).
 - [5] C. W. Beenakker, *Rev. Mod. Phys.* **69**, 731 (1997).
 - [6] S. Sorathia, F. M. Izrailev, V. G. Zelevinsky, and G. L. Celardo, *Phys. Rev. E* **86**, 011142 (2012).
 - [7] A. Ziletti, F. Borgonovi, G. L. Celardo, F. M. Izrailev, L. Kaplan, and V. G. Zelevinsky, *Phys. Rev. B* **85**, 052201 (2012).
 - [8] G. Vattay, D. Salahub, I. Csabai, A. Nassimi, and S. A. Kaufmann, *J. of Phys.: Conf. Ser.* **626**, 012023 (2015).
 - [9] J. Cao and G. A. Voth, *J. Chem. Phys.* **100**, 5106 (1994).
 - [10] J. Grad, G. Hernandez, and S. Mukamel, *Phys. Rev. A* **37**, 3835 (1988).
 - [11] G. L. Celardo, F. Borgonovi, M. Merkli, V. I. Tsifrinovich, and G. P. Berman, *J. Phys. Chem. C* **116**,

- 22105 (2012).
- [12] F. Caruso, S. F. Huelga, and M. B. Plenio, *Phys. Rev. Lett.* **105**, 190501 (2010).
 - [13] F. C. Spano, J. R. Kuklinski, and S. Mukamel, *J. Chem. Phys.* **94**, 7534 (1991).
 - [14] R. Monshouwer, M. Abrahamsson, F. Van Mourik, and R. Van Grondelle, *J. Phys. Chem. B* **101**, 7241 (1997).
 - [15] M. Mohseni, P. Rebentrost, S. Lloyd, and A. Aspuru-Guzik, *J. Chem. Phys.* **129**, 11B603 (2008).
 - [16] D. Ferrari, G. Celardo, G. P. Berman, R. Sayre, and F. Borgonovi, *J. Phys. Chem. C* **118**, 20 (2014).
 - [17] F. Mattiotti, W. M. Brown, N. Piovella, S. Olivares, E. M. Gauger, and G. L. Celardo, *New J. Phys.* **23**, 103015 (2021).
 - [18] J. Schachenmayer, C. Genes, E. Tignone, and G. Pupillo, *Phys. Rev. Lett.* **114**, 196403 (2015).
 - [19] N. C. Chávez, F. Mattiotti, J. A. Méndez-Bermúdez, F. Borgonovi, and G. L. Celardo, *Phys. Rev. Lett.* **126**, 153201 (2021).
 - [20] F. Mattiotti, M. Sarovar, G. G. Giusteri, F. Borgonovi, and G. L. Celardo, *New J. Phys.* **24**, 013027 (2022).
 - [21] C. D. Bostick, S. Mukhopadhyay, I. Pecht, M. Sheves, D. Cahen, and D. Lederman, *Rep. Prog. Phys.* **81**, 026601 (2018).
 - [22] R. Gutierrez, E. Díaz, R. Naaman, and G. Cuniberti, *Phys. Rev. B* **85**, 081404(R) (2012).
 - [23] M. Gullì, A. Valzelli, F. Mattiotti, M. Angeli, F. Borgonovi, and G. L. Celardo, *New J. Phys.* **21**, 013019 (2019).
 - [24] C. Chuang, C. K. Lee, J. M. Moix, J. Knoester, and J. Cao, *Phys. Rev. Lett.* **116**, 196803 (2016).
 - [25] L. Sepunaru, I. Pecht, M. Sheves, and D. Cahen, *J. Am. Chem. Soc.* **133**, 2421 (2011).
 - [26] S. Sahu, S. Ghosh, B. Ghosh, K. Aswani, K. Hirata, D. Fujita, and A. Bandyopadhyay, *Biosens. Bioelectron.* **47**, 141 (2013).
 - [27] G. Celardo, M. Angeli, and T. Craddock, *New J. Phys.* **21**, 023005 (2019).
 - [28] P. W. Anderson, *Phys. Rev.* **109**, 1492 (1958).
 - [29] P. W. Anderson, *Rev. Mod. Phys.* **50**, 191 (1978).
 - [30] E. Abrahams, P. W. Anderson, D. C. Licciardello, and T. V. Ramakrishnan, *Phys. Rev. Lett.* **42**, 673 (1979).
 - [31] S. Aubry and G. André, *Ann. Israel Phys. Soc.* **3**, 133 (1980).
 - [32] D. H. Dunlap, H.-L. Wu, and P. W. Phillips, *Phys. Rev. Lett.* **65**, 88 (1990).
 - [33] F. M. Izrailev and A. A. Krokhin, *Phys. Rev. Lett.* **82**, 4062 (1999).
 - [34] A. D. Mirlin, Y. V. Fyodorov, F.-M. Dittes, J. Quezada, and T. H. Seligman, *Phys. Rev. E* **54**, 3221 (1996).
 - [35] R. Landauer, *Phil. Mag.* **21**, 863 (1970).
 - [36] N. F. Mott, *Rev. Mod. Phys.* **40**, 677 (1968).
 - [37] N. F. Mott, *Rev. Mod. Phys.* **50**, 203 (1978).
 - [38] H. Haken, *Fortschritte Phys.* **6**, 271–334 (1958).
 - [39] M. Büttiker, *Phys. Rev. B* **33**, 3020 (1986).
 - [40] J. L. D’Amato and H. M. Pastawski, *Phys. Rev. B* **41**, 7411 (1990).
 - [41] H. M. Pastawski, *Phys. Rev. B* **44**, 6329 (1991).
 - [42] H. M. Pastawski and G. Usaj, *Phys. Rev. B* **57**, 5017 (1998).
 - [43] D. J. Thouless and S. Kirkpatrick, *J. Phys. C: Sol. St. Phys.* **14**, 235 (1981).
 - [44] F. Caruso, A. W. Chin, A. Datta, S. F. Huelga, and M. B. Plenio, *J. Chem. Phys.* **131**, 09B612 (2009).
 - [45] Y. Zhang, G. L. Celardo, F. Borgonovi, and L. Kaplan, *Phys. Rev. E* **96**, 052103 (2017).
 - [46] A. R. Coates, B. W. Lovett, and E. M. Gauger, *New J. Phys.* **23**, 123014 (2021).
 - [47] J. M. Moix, M. Khasin, and J. Cao, *New J. Phys.* **15**, 085010 (2013).
 - [48] C. Chuang, C. K. Lee, J. M. Moix, J. Knoester, and J. Cao, *Phys. Rev. Lett.* **116**, 196803 (2016).
 - [49] A. M. Lacerda, J. Gould, and G. T. Landi, *Phys. Rev. B* **104**, 174203 (2021).
 - [50] D. Dwiputra and F. P. Zen, *Phys. Rev. A* **104**, 022205 (2021).
 - [51] R. A. Molina, E. Benito-Matias, A. D. Somoza, L. Chen, and Y. Zhao, *Phys. Rev. E* **93**, 022414 (2016).
 - [52] G. L. Celardo, G. G. Giusteri, and F. Borgonovi, *Phys. Rev. B* **90**, 075113 (2014).
 - [53] B. Zhang, W. Song, P. Pang, Y. Zhao, P. Zhang, I. Csabai, G. Vattay, and S. Lindsay, *Nano Futures* **1**, 035002 (2017).
 - [54] B. Zhang, W. Song, P. Pang, H. Lai, Q. Chen, P. Zhang, and S. Lindsay, *Proc. Natl. Acad. Sci. U.S.A.* **116**, 5886 (2019).
 - [55] S. Kauffman, *Act. Nerv. Super.* **61**, 61 (2019).
 - [56] S. Kauffman, S. Niranen, and G. Vattay, *Uses of systems with degrees of freedom posed between fully quantum and fully classical states*, U.S. Patent No. 2012/0071333 A1 (2012).
 - [57] G. Vattay, S. Kauffman, and S. Niiranen, *PLoS ONE* **9**, e89017 (2014).
 - [58] E. J. Torres-Herrera and L. F. Santos, *Phil. Trans. R. Soc. A* **375**, 20160434 (2017).
 - [59] S. Xu, X. Li, Y.-T. Hsu, B. Swingle, and S. Das Sarma, *Phys. Rev. Res.* **1**, 032039(R) (2019).
 - [60] F. S. Lozano-Negro, P. R. Zangara, and H. M. Pastawski, *Chaos Solit. Fractals* **150**, 111175 (2021).
 - [61] A. S. Aramthottil, T. Chanda, P. Sierant, and J. Zakrzewski, *Phys. Rev. B* **104**, 214201 (2021).
 - [62] U. Kuhl, F. M. Izrailev, A. A. Krokhin, and H.-J. Stockmann, *Appl. Phys. Lett.* **77**, 633 (2000).
 - [63] G. Roati, C. D’Errico, L. Fallani, M. Fattori, C. Fort, M. Zaccanti, G. Modugno, M. Modugno, and M. Inguscio, *Nature* **453**, 895 (2008).
 - [64] M. Schreiber, S. S. Hodgman, P. Bordia, H. P. Lüschen, M. H. Fischer, R. Vosk, E. Altman, U. Schneider, and I. Bloch, *Science* **349**, 842 (2015).
 - [65] P. Bordia, H. Lüschen, U. Schneider, M. Knap, and I. Bloch, *Nat. Phys.* **13**, 460 (2017).
 - [66] S. Ostlund, R. Pandit, D. Rand, H. J. Schellnhuber, and E. D. Siggia, *Phys. Rev. Lett.* **50**, 1873 (1983).
 - [67] J. F. Weisz and H. M. Pastawski, *Phys. Lett. A* **105**, 421 (1984).
 - [68] G. Domínguez-Castro and R. Paredes, *Eur. J. Phys.* **40**, 045403 (2019).
 - [69] See Supplemental Material at [URL_will_be_inserted_by_publisher](#) for detailed calculations and supplemental results, including Refs. [127–133].
 - [70] J. Sokoloff, *Phys. Rep.* **126**, 189 (1985).
 - [71] H. Haken and G. Strobl, *Z Phys. A-Hadron Nucl.* **262**, 135 (1973).
 - [72] P. Reineker, Stochastic Liouville equation approach: Coupled coherent and incoherent motion, optical line shapes, magnetic resonance phenomena, in *Exciton Dynamics in Molecular Crystals and Aggregates* (Springer, Berlin, Heidelberg, 1982) pp. 111–226.

- [73] K. Fujimoto, R. Hamazaki, and Y. Kawaguchi, *Phys. Rev. Lett.* **129**, 110403 (2022).
- [74] C. J. Cattena, R. A. Bustos-Marín, and H. M. Pastawski, *Phys. Rev. B* **82**, 144201 (2010).
- [75] L. J. Fernández-Alcázar and H. M. Pastawski, *Phys. Rev. A* **91**, 022117 (2015).
- [76] J. Strümpfer, M. Sener, and K. Schulten, *J. Phys. Chem. Lett.* **3**, 536 (2012).
- [77] S. Lloyd, M. Mohseni, A. Shabani, and H. Rabitz, arXiv preprint arXiv:1111.4982 [10.48550/arXiv.1111.4982](#) (2011).
- [78] H. M. Pastawski, *Phys. Rev. B* **46**, 4053 (1992).
- [79] G. A. Álvarez, E. P. Danieli, P. R. Levstein, and H. M. Pastawski, *Phys. Rev. A* **75**, 062116 (2007).
- [80] H. Hiramoto and S. Abe, *J. Phys. Soc. Jap.* **57**, 1365 (1988).
- [81] R. Fleischmann, T. Geisel, R. Ketzmerick, and G. Petschel, *Phys. D: Nonlinear Phenom.* **86**, 171 (1995).
- [82] A. Purkayastha, S. Sanyal, A. Dhar, and M. Kulkarni, *Phys. Rev. B* **97**, 174206 (2018).
- [83] P. R. Levstein, H. M. Pastawski, and J. L. D'Amato, *J. Phys. Condens. Matter* **2**, 1781 (1990).
- [84] J. Dalibard, Y. Castin, and K. Mølmer, *Phys. Rev. Lett.* **68**, 580 (1992).
- [85] H. J. Carmichael, *Phys. Rev. Lett.* **70**, 2273 (1993).
- [86] P. R. Levstein, H. M. Pastawski, and R. Calvo, *J. Phys. Condens. Matter* **3**, 1877 (1991).
- [87] H. M. Pastawski, G. Usaj, and P. R. Levstein, in *Some Contemporary Problems of Condensed Matter Physics*, edited by S. J. Vlaev and L. M. Gaggero Sager (NOVA Science, New York, 2001) pp. 223–258.
- [88] R. A. Jalabert and H. M. Pastawski, *Phys. Rev. Lett.* **86**, 2490 (2001).
- [89] F. M. Cucchietti, D. A. R. Dalvit, J. P. Paz, and W. H. Zurek, *Phys. Rev. Lett.* **91**, 210403 (2003).
- [90] L. Fallani, J. E. Lye, V. Guarrera, C. Fort, and M. Inguscio, *Phys. Rev. Lett.* **98**, 130404 (2007).
- [91] L. Fallani, C. Fort, and M. Inguscio, *Adv. At. Mol. Opt. Phys.* **56**, 119 (2008).
- [92] L. Fallani private communication.
- [93] R. Merlin, K. Bajema, R. Clarke, F. Y. Juang, and P. K. Bhattacharya, *Phys. Rev. Lett.* **55**, 1768 (1985).
- [94] V. K. Varma and M. Žnidarič, *Phys. Rev. B* **100**, 085105 (2019).
- [95] A. D. Mirlin and F. Evers, *Phys. Rev. B* **62**, 7920 (2000).
- [96] E. Cuevas, V. Gasparian, and M. Ortuño, *Phys. Rev. Lett.* **87**, 056601 (2001).
- [97] J. A. Mendez-Bermudez, A. Alcazar-Lopez, and I. Varga, *EPL* **98**, 37006 (2012).
- [98] E. Ott, T. M. Antonsen, and J. D. Hanson, *Phys. Rev. Lett.* **53**, 2187 (1984).
- [99] F. M. Cucchietti and H. M. Pastawski, *Phys. A* **283**, 302 (2000).
- [100] H. M. Pastawski, J. F. Weisz, and E. A. Albanesi, *Phys. Rev. B* **52**, 10665 (1995).
- [101] R. Gutiérrez, S. Mandal, and G. Cuniberti, *Phys. Rev. B* **71**, 235116 (2005).
- [102] D. Nozaki, C. Gomes da Rocha, H. M. Pastawski, and G. Cuniberti, *Phys. Rev. B* **85**, 155327 (2012).
- [103] S. Reineke, M. Thomschke, B. Lüssem, and K. Leo, *Reviews of Modern Physics* **85**, 1245 (2013).
- [104] K. Namsheer and C. S. Rout, *RSC Advances* **11**, 5659 (2021).
- [105] P. Peng, B. Ye, N. Y. Yao, and P. Cappellaro, *Nat. Phys.*, 1 (2023).
- [106] E. Rufeil-Fiori, C. M. Sánchez, F. Y. Oliva, H. M. Pastawski, and P. R. Levstein, *Phys. Rev. A* **79**, 032324 (2009).
- [107] H. M. Pastawski, G. Usaj, and P. R. Levstein, *Chem. Phys. Lett.* **261**, 329 (1996).
- [108] Z. Mádi, B. Brutscher, T. Schulte-Herbrüggen, R. Brüschweiler, and R. Ernst, *Chem. Phys. Lett.* **268**, 300 (1997).
- [109] E. O'Brien, M. E. Holt, M. K. Thompson, L. E. Salay, A. C. Ehlinger, W. J. Chazin, and J. K. Barton, *Science* **355**, 6327 (2017).
- [110] C.-T. Shih, S. Roche, and R. A. Römer, *Phys. Rev. Lett.* **100**, 018105 (2008).
- [111] M. Saki and A. Prakash, *Free Radic. Biol. Med.* **107**, 216 (2017).
- [112] Q. Lu, D. Bhat, D. Stepanenko, and S. Pigolotti, *Phys. Rev. Lett.* **127**, 208102 (2021).
- [113] R. Szabla, M. Zdrowowicz, P. Spisz, N. J. Green, P. Stadlbauer, H. Kruse, J. Šponer, and J. Rak, *Nat. Comm.* **12**, 3018 (2021).
- [114] G. Rosenblum, N. Elad, H. Rozenberg, F. Wiggers, J. Jungwirth, and H. Hofmann, *Nat. Commun.* **12**, 2967 (2021).
- [115] R. E. Blankenship, *Molecular mechanisms of photosynthesis - Chapter 6* (John Wiley & Sons, 2021).
- [116] J. R. Winkler and H. B. Gray, *Chem. Rev.* **114**, 3369 (2013).
- [117] S. M. Sarhangi and D. V. Matyushov, *ACS Omega* **8**, 27355 (2023).
- [118] D. Wang, O. C. Fiebig, D. Harris, H. Toporik, Y. Ji, C. Chuang, M. Nairat, A. L. Tong, J. I. Ogren, S. M. Hart, *et al.*, *Proc. Natl. Acad. Sci. U.S.A.* **120**, e2220477120 (2023).
- [119] J. Cao, R. J. Cogdell, D. F. Coker, H.-G. Duan, J. Hauer, U. Kleinekathöfer, T. L. C. Jansen, T. Mančal, R. J. D. Miller, J. P. Ogilvie, V. I. Prokhorenko, T. Renger, H.-S. Tan, R. Tempelaar, M. Thorwart, E. Thyryhaug, S. Westenhoff, and D. Zigmantas, *Sci. Adv.* **6**, eaaz4888 (2020).
- [120] A. Jain, J. Gosling, S. Liu, H. Wang, E. M. Stone, S. Chakraborty, P.-S. Jayaraman, S. Smith, D. B. Amabilino, M. Fromhold, Y. Long, L. Pérez-García, L. Turyanska, R. Rahman, and F. J. Rawson, *Nat. Nanotechnol.* [10.1038/s41565-023-01496-y](#) (2023).
- [121] H. M. Pastawski, L. F. Torres, and E. Medina, *Chem. Phys.* **281**, 257 (2002).
- [122] E. Santos, M. T. M. Koper, and W. Schmickler, *Chem. Phys. Lett.* **419**, 421 (2006).
- [123] A. Nitzan, *Chemical dynamics in condensed phases: relaxation, transfer and reactions in condensed molecular systems* (Oxford university press, 2006).
- [124] M. Peralta, S. Feijoo, S. Varela, R. Gutierrez, G. Cuniberti, V. Mujica, and E. Medina, *J. Chem. Phys.* **159**, 024711 (2023).
- [125] A. I. Larkin and Y. N. Ovchinnikov, *J. Exp. Theor. Phys.* **28**, 1200 (1969).
- [126] R. B. Laughlin, *Nucl. Phys. B - Proc. Suppl.* **2**, 213 (1987).
- [127] T. Botzung, D. Hagenmüller, S. Schütz, J. Dubail, G. Pupillo, and J. Schachenmayer, *Phys. Rev. B* **102**, 144202 (2020).

- [128] Y. Zhang, G. L. Celardo, F. Borgonovi, and L. Kaplan, [Phys. Rev. E **95**, 022122 \(2017\)](#).
- [129] H. De Raedt and B. De Raedt, [Phys. Rev. A **28**, 3575 \(1983\)](#).
- [130] D. J. Thouless, [Phys. Rev. B **28**, 4272 \(1983\)](#).
- [131] F. Evers and A. D. Mirlin, [Phys. Rev. Lett. **84**, 3690 \(2000\)](#).
- [132] F. Evers and A. D. Mirlin, [Rev. Mod. Phys. **80**, 1355 \(2008\)](#).
- [133] C. Chiaracane, A. Purkayastha, M. T. Mitchison, and J. Goold, [Phys. Rev. B **105**, 134203 \(2022\)](#).

Supplementary Material – Universal stability of coherently diffusive 1D systems with respect to decoherence.

CONTENTS

Acknowledgments	5
References	5
I. Current.	S1
A. Steady-state current: Average transfer time method.	S2
1. Heuristic construction of the mean transfer time.	S2
II. The Quantum Drift Model	S3
III. HHAA model: dynamics in absence of dephasing.	S3
A. Extended phase.	S4
B. Critical point.	S4
IV. Diffusion coefficient in presence of decoherence.	S5
A. Green-Kubo formula.	S5
B. Analytical expression of the Diffusion coefficient from the coherent dynamics.	S6
1. Analytical solution for the spreading.	S8
C. Analytical expression of the Diffusion coefficient in the limit of strong and weak dephasing.	S8
1. Large dephasing.	S9
2. Extended phase ($W < 2J$).	S10
3. MIT ($W = 2J$).	S10
4. Localized phase ($W > 2J$).	S10
V. HHAA model with different values of q .	S11
VI. Study of different paradigmatic models of transport.	S11
A. The Fibonacci chain.	S12
B. The PBRM model.	S13
VII. Purity.	S14

I. CURRENT.

In this section we study the steady-state current through the HHAA model in presence of pumping and draining of excitation from the opposite edges of the chain, in presence of dephasing. We also derive an approximate expression of the current as a function of the diffusion coefficient.

To generate a current, excitations are incoherently pumped and drained at the chain edges. This is modeled by including additional terms in the Lindblad master equation Eq. (2) from the main text, which becomes

$$\dot{\rho} = \mathcal{L}[\rho] = -\frac{i}{\hbar} [H\rho - \rho H] + \mathcal{L}_\phi[\rho] + \mathcal{L}_p[\rho] + \mathcal{L}_d[\rho], \quad (\text{S1})$$

where H is the HHAA Hamiltonian (1) from the main text, \mathcal{L}_ϕ is the dephasing dissipator Eq. (3) from the main text, while the additional terms,

$$\mathcal{L}_p[\rho] = \frac{\gamma_p}{\hbar} \left(|1\rangle \langle 0| \rho |0\rangle \langle 1| - \frac{1}{2} |0\rangle \langle 0| \rho - \frac{1}{2} \rho |0\rangle \langle 0| \right), \quad (\text{S2})$$

and

$$\mathcal{L}_d[\rho] = \frac{\gamma_d}{\hbar} \left(|0\rangle \langle N| \rho |N\rangle \langle 0| - \frac{1}{2} |N\rangle \langle N| \rho - \frac{1}{2} \rho |N\rangle \langle N| \right), \quad (\text{S3})$$

are two operators modeling the pumping on the first site ($|1\rangle$) and draining from the last site ($|N\rangle$). Here $|0\rangle$ is the vacuum state, where no excitation is present in the system [19, 127]. For simplicity, here the pumping and draining rates are set to be equal in magnitude ($\gamma_p = \gamma_d$). From solving Eq. (S1) at the steady-state ($\mathcal{L}[\rho_{ss}] = 0$) one can compute the stationary current,

$$I_{ss} = \frac{\gamma_d}{\hbar} \langle N | \rho_{ss} | N \rangle. \quad (\text{S4})$$

with ρ_{ss} being the steady-state density operator [19, 127].

A. Steady-state current: Average transfer time method.

Since the master equation approach discussed above is numerically expensive, for large N we use the *average transfer time* method (ATT), as described in [19]. The average transfer time τ is defined as

$$\tau = \frac{\gamma_d}{\hbar} \int_0^\infty t \langle N | \exp(-\mathcal{L}_{\text{eff}} t) \rho(0) | N \rangle dt = \frac{\gamma_d}{\hbar} \langle N | \mathcal{L}_{\text{eff}}^{-2} \rho(0) | N \rangle. \quad (\text{S5})$$

where \mathcal{L}_{eff} is the one from Eq. (S1) *without pumping*. In [19] it has been proved that the steady-state current determined from the master equation (S1) *in absence of dephasing* depends only on the average transfer time, namely

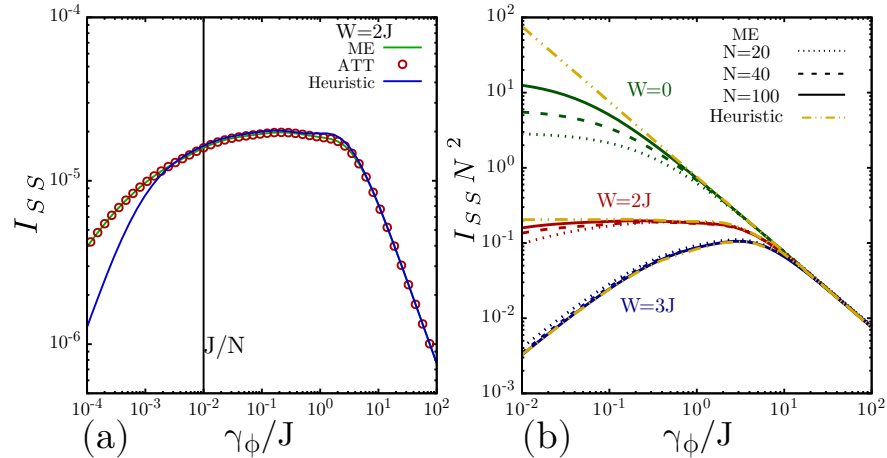
$$I_{ss} = \frac{\gamma_p}{\gamma_p \tau + \hbar}. \quad (\text{S6})$$

We have numerically verified that Eq. (S6) is valid also in presence of dephasing, so in the following we use it due to its lower numerical complexity together with a heuristic construction, detailed here below.

1. Heuristic construction of the mean transfer time.

The ATT method gives us the possibility to heuristically construct the mean transfer time by considering the characteristic times of dephasing-induced diffusion and draining.

Since at equilibrium the probability of being at site N is $1/N$ and the drain rate is γ_d/\hbar , we can estimate the drainage time as $\hbar N/\gamma_d$. Then, in order to determine the diffusion time, we know that an excitation moves from one site to a neighbor with an average time $a^2/(2D)$. Furthermore, the excitation moves as a random walk and the total



SUPPLEMENTARY FIG. S1. (a) Steady-state current vs. γ_ϕ/j for the HHAA model for $N = 100$ and $W = 2J$ obtained with three different methods: (i) Master equation (ME), (ii) average transfer time method (ATT) and (iii) heuristic expression, see Eq. (S7)). (b) Rescaled steady state current $I_{SS} N^2$ as a function of dephasing (γ_ϕ/J) in the extended, critical, and localized regime for different system's sizes $N = \{20, 40, 100\}$. $I_{SS} N^2$ is calculated using the ME method and shown with different dash types. The diffusion coefficient based (Heuristic) estimation of the current for $N = 1000$ is included with yellow dot-dashed lines.

number of steps required in 1D is $N(N-1)$. Therefore, we estimate the diffusion time as $N(N-1)a^2/(2D)$ [45, 128]. Thus, adding the drainage time and the diffusion time we have

$$\tau = \hbar \frac{N}{\gamma_d} + \frac{(N-1)N}{2D} a^2. \quad (\text{S7})$$

Figure S1a shows a comparison of I_{ss} as a function of dephasing computed using the three different methods illustrated above here: the stationary solution of the master equation (S1) (ME), the ATT method (S5-S6), and the heuristic formula (S7). In the latter case, the diffusion coefficient D has been computed using the Green-Kubo approach [Eq. (S20), Sup. Mat. IV A]. A general good agreement is observed between the three approaches. Deviations at small dephasing are due to the finite system size ($N = 100$), for which the excitation reaches the chain edge ballistically within a time shorter than $\tau_\phi = \hbar/\gamma_\phi$.

Fig. S1b shows the normalized steady-state current $N^2 I_{ss}$ as a function of γ_ϕ for different N in the three regimes for the HHAA model described in the main text. We observe that, as the length N of the chain is increased, the behavior of the current is determined by the diffusion coefficient Eq. (S7) (see yellow lines in Fig. 2b) where D has been computed analytically for $W = 0$ (SM Eq. (S35)) and numerically via the quantum drift approach for $W \neq 0$ and $N = 1000$ (see Sec. II). The current decreases with dephasing in the extended regime ($W = 0$) and it is enhanced in the localized regime ($W = 3J$, up to an optimal dephasing), while it remains almost unaffected at the critical point ($W = 2J$) up to a characteristic dephasing.

Although this analysis is done for the HHAA model, it should also be valid for other models with nearest-neighbor couplings, such as the Fibonacci chain analyzed in this paper. In other words, we expect that the steady-state current is mostly determined by the diffusion coefficient in such systems.

II. THE QUANTUM DRIFT MODEL

In order to reduce the computational cost of calculation of the dynamics in presence of decoherence we use the Quantum Drift (QD) model, which only involves Trotter-Suzuki evolution of the wave-vector [75, 129] under uncorrelated local noise. Here, the dynamics are obtained by the sequential application of unitary evolution operators to the wave-function in small time steps (dt). The noise/decoherence (interaction with the environment), is introduced by adding stochastic energies fluctuations on every site, $\hat{\Gamma}_\phi = \sum_n \beta_n |n\rangle \langle n|$, uncorrelated in time. The probability distribution of these fluctuations is a Lorentzian function,

$$P(\beta_n) = \frac{1}{\pi} \frac{\frac{\gamma_\phi}{2}}{\beta_n^2 + (\frac{\gamma_\phi}{2})^2}. \quad (\text{S8})$$

Thus, the unitary evolution in a small time step dt is:

$$\hat{U}(dt) \approx e^{i\hat{\Gamma}_\phi dt/\hbar} e^{-i\hat{\mathcal{H}} dt/\hbar}, \quad (\text{S9})$$

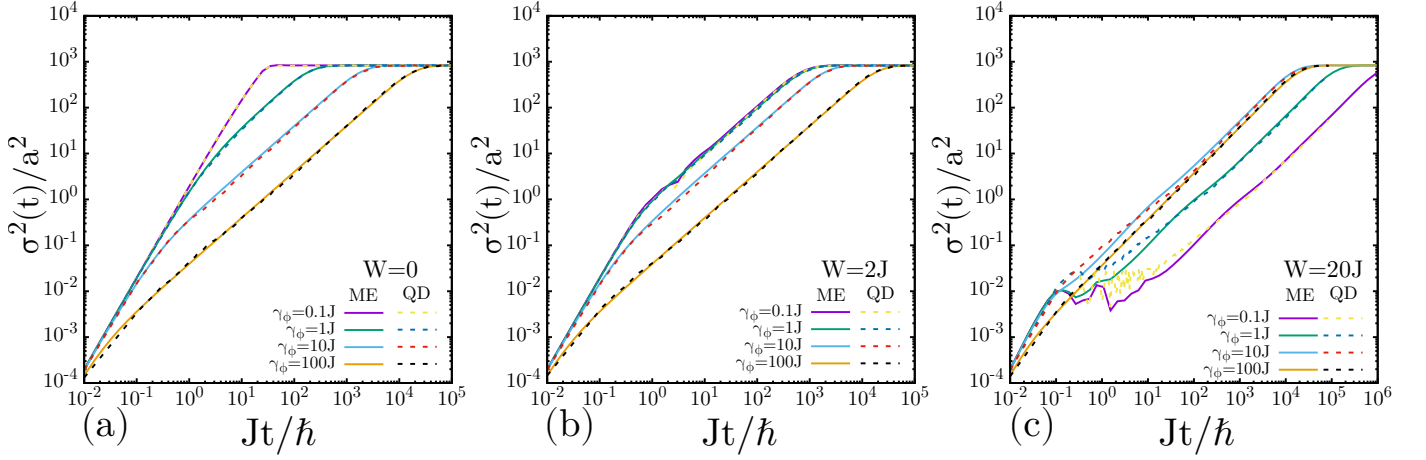
where $\hat{\mathcal{H}}$ is the system's Hamiltonian. Finally, the evolved wave function at time $t = N_t dt$ is:

$$|\hat{\psi}(t)\rangle = \prod_{j=1}^{N_t} e^{i\hat{\Gamma}_\phi dt/\hbar} e^{-i\hat{\mathcal{H}} dt/\hbar} |\psi(0)\rangle. \quad (\text{S10})$$

The QD evolution described here is equivalent to the Haken-Strobl dephasing (Eq. (3)), see Fig. S2. As one can see there is a very good agreement between the Lindbladian and the QD evolution of the second moment of an initially local excitation for different dephasing strengths and system parameters.

III. HHAA MODEL: DYNAMICS IN ABSENCE OF DEPHASING.

Here, we study the spreading of an initially localized wave packet at the center of the HHAA chain in absence of dephasing. In particular, we focus on the time evolution of the second moment σ_0^2 of the probability distribution to find the particle along the chain in absence of decoherence. As shown in the main text, in absence of decoherence and for long enough times, the second moment grows ballistically for $W < 2J$, diffusively for $W = 2J$ and saturates for $W > 2J$ [81].



SUPPLEMENTARY FIG. S2. Spreading of excitation for the HHAA model. Initial state a single site in the middle of the chain. Solid curves: Pure dephasing Haken-Strobl from a Lindbladian evolution (ME). Dashed curves: Quantum drift (QD) simulation. The parameters are $N = 100$, (a) $W = 0$, (b) $W = 2J$ and (c) $W = 20J$.

It is known that, in the HHAA, in the localized regime the localization length of all eigenfunctions is $2\xi = a/\ln[W/2J]$ [31, 80, 81]. It follows that the wave packet probability distribution at the steady state is localized close to a site n_0 , $P(n) = |\langle n|\psi(t)\rangle|^2 = \frac{1}{2\xi}(e^{-|n-n_0|/\xi})$. Therefore, the variance's saturation value will be $\lim_{t \rightarrow \infty} \sigma_0^2(t) = l^2 = 2\xi^2 = 2a^2(2\ln(W/2J))^{-2}$. In the following we will characterize the dynamics in the different regimes.

A. Extended phase.

In the extended phase, the dynamics of the variance for very long times become ballistic, $\sigma_0^2(t) = u^2 t^2$. From the Hamiltonian [Eq. (1) of the main text] in the cases $q = 0$ (ordered chain) and $q = 1/2$ (dimerized chain) we have proved analytically (not shown) that the velocity u is directly connected with the support B of the spectral bands, and we have $u^2 = \frac{a^2 B^2}{8\hbar^2}$. For $q = 0$ there is a single band, $B = 4J$ and for $q = 1/2$ we have two bands, with $B = 2\sqrt{W^2 + 4J^2} - 2\sqrt{W^2}$.

We here conjecture that the same expression is valid for any value of q in the HHAA model. For q given by the golden mean, in Ref. [130] it was shown that $B = 2|2J - W|$. Thus we have $u^2 = 4a^2|2J - W|^2$ and the behavior of the variance in for long times is given by:

$$\sigma_0^2(t) = \frac{a^2|2J - W|^2}{2\hbar^2} t^2.$$

These results have been confirmed numerically in Fig. 2a in the main text.

B. Critical point.

Here we analytically estimate the diffusion coefficient in absence of decoherence. We calculate the spreading of the wave packet $\psi(t)$ perturbatively for short times (before the scattering due to the site potential enters in the dynamics), so that the probability to be at site n at time t is: $P_n(t) = |\langle n|\psi(t)\rangle|^2 \simeq |\langle n|(1 - i\mathcal{H}t/\hbar)|n_0\rangle|^2$, where n_0 is the site where the excitation is localized initially. Defining $\mathcal{H}_{n,n_0} = \langle n|\mathcal{H}|n_0\rangle$, and considering without loss of generality, $n_0 = 0$, we can write:

$$\sigma_0^2(t) = a^2 \sum_n P_n(t) n^2 - a^2 \left(\sum_n P_n(t) n \right)^2 \quad (\text{S11})$$

$$\approx (t/\hbar)^2 a^2 \sum_n \mathcal{H}_{n,0}^2 n^2 - a^2 (t/\hbar)^4 \sum_n \mathcal{H}_{n,0}^4 n^2 \quad (\text{S12})$$

$$\approx (t/\hbar)^2 a^2 \sum_n \mathcal{H}_{n,0}^2 n^2 = v_0^2 t^2 \quad (\text{S13})$$

from which we find:

$$v_0^2 = 2a^2(J/\hbar)^2, \quad (\text{S14})$$

for the HHAA since there are only nearest neighbors interactions.

We may define a time scale where the initial ballistic spreading end due to the presence of a quasi-periodic site potential of magnitude W . To see this effect, the perturbation expansion needs to be carry out to the 4th order: $P_n(t) = |\langle n|\psi(t)\rangle|^2 \simeq |\langle n|(1 - i\mathcal{H}t/\hbar - \frac{1}{2}\mathcal{H}^2t^2/\hbar - i\frac{1}{6}\mathcal{H}^3t^3/\hbar + \frac{1}{24}\mathcal{H}^4t^4/\hbar)|n_0\rangle|^2$. Thus, to this level of approximation we have:

$$\begin{aligned} \sigma_0^2(t)/a^2 &\approx 2J^2(t/\hbar)^2 - \frac{1}{12}((\mathcal{H}_{0,0} - \mathcal{H}_{1,1})^2 + (\mathcal{H}_{0,0} - \mathcal{H}_{-1,-1})^2)J^2(t/\hbar)^4, \\ \sigma_0^2(t)/a^2 &\approx 2J^2(t/\hbar)^2 - \frac{2}{12}\langle(\mathcal{H}_{n,n} - \mathcal{H}_{n+1,n+1})^2\rangle J^2(t/\hbar)^4. \end{aligned}$$

where the energy differences squared were replaced by the average value:

$$(\Delta E)^2 = \langle(\mathcal{H}_{n,n} - \mathcal{H}_{n+1,n+1})^2\rangle = \frac{1}{N-1} \sum_{n=1}^{N-1} \frac{(\mathcal{H}_{n,n} - \mathcal{H}_{n+1,n+1})^2}{2}. \quad (\text{S15})$$

This definition takes into account the ‘‘correlation’’ between neighbors. For the HHAA model the average can be taken over the sites n or the realizations of the potential (phase θ in Eq. 1). For independent random disorder (Anderson disorder), yields directly the variance of the disorder $((\Delta E)^2 = \frac{1}{N-1} \sum_{n=1}^{N-1} \mathcal{H}_{n,n}^2)$, which is the standard magnitude to calculate the disorder time scale.

The first effect of this quartic correction is to change the concavity of the $\sigma_0^2(t)$. This will happen when the second derivative of $\sigma_0^2(t)/a^2$ vanish at a time τ_W , so that:

$$\tau_W = \sqrt{\left(\frac{\langle(\mathcal{H}_{n,n} - \mathcal{H}_{n+1,n+1})^2\rangle}{2\hbar^2}\right)^{-1}} = \frac{\hbar}{\Delta E}. \quad (\text{S16})$$

By replacing with the HHAA site energies, using trigonometric identities, and summing over the sites, it can be shown that $\Delta E = W\sqrt{(1 - \cos(2\pi q))/2}$, and we have:

$$\tau_W = \frac{\sqrt{2}\hbar}{W\sqrt{(1 - \cos(2\pi q))}}, \quad (\text{S17})$$

then, the diffusion coefficient in absence of dephasing, D_0 , can be computed as follows:

$$D_0 = \frac{v_0^2\tau_W}{2} = \frac{a^2J^2}{\hbar} \frac{\sqrt{2}}{W\sqrt{(1 - \cos(2\pi q))}}. \quad (\text{S18})$$

It is interesting to note how the correlations of the model (given by the modulation wave vector q) influence the scattering times and therefore the diffusion $\sigma_0^2(t) = 2D_0t = v_0^2\tau_W t$.

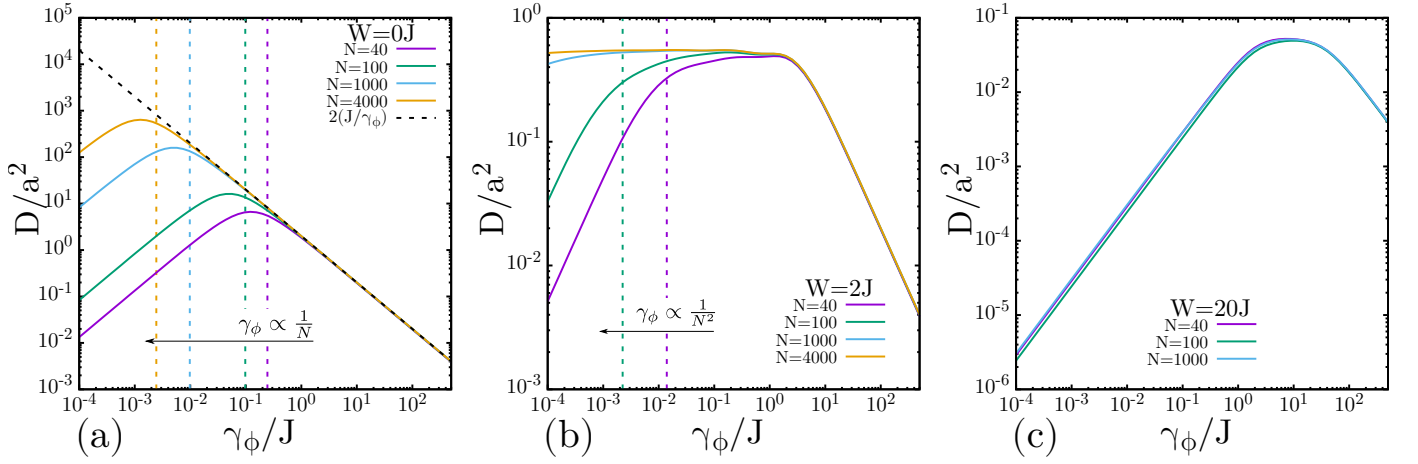
Notice that here, the potential strength enters with a different power law than in the mean-free-time between collisions that results from the application of the Fermi Golden Rule to a Bloch state of energy ε for the *uncorrelated disorder* of Anderson’s model[43] $1/\tau_{FGR} = (2\pi/\hbar)(W^2/12)N_1(\varepsilon)$ with $N_1(\varepsilon) \propto 1/4\pi J\sqrt{1 - (\varepsilon/2J)^2}$ being the density of directly connected states.

IV. DIFFUSION COEFFICIENT IN PRESENCE OF DECOHERENCE.

A. Green-Kubo formula.

The diffusion coefficient D in presence of decoherence for the Haken-Strobl model can be computed from the Green-Kubo expression, using only the eigenenergies and eigenstates of the Hamiltonian,

$$\mathcal{H}\phi^\mu = \varepsilon_\mu\phi^\mu \quad (\text{S19})$$



SUPPLEMENTARY FIG. S3. Diffusion coefficient D/a^2 , calculated using the Green-Kubo approach (Eq. (S20)), vs. γ_ϕ/J for the HHAA model with Haken-Strobl dephasing for different values of $N = \{40, 100, 1000, 4000\}$. Figure (a) is for $W/J = 0$ (metallic regime), figure (b) is for $W/J = 2.0$ (MIT regime), and figure (c) is for $W/J = 20$ (insulator regime). Vertical dashed lines indicate the values of γ_ϕ below which finite size effects are relevant. The dependence of this value with N is shown on top of the black arrow.

as it has been derived in Ref. [48]:

$$D(\vec{u}) = \frac{\hbar}{N} \sum_{\mu, \nu=1}^N \frac{\gamma_\phi}{\gamma_\phi^2 + \omega_{\mu, \nu}^2} |\hat{j}_{\mu, \nu}(\vec{u})|^2, \quad (\text{S20})$$

where γ_ϕ is the dephasing strength, $\omega_{\mu, \nu} = \varepsilon_\mu - \varepsilon_\nu$ is the energy difference between eigenstates μ and ν , and $\hat{j}_{\mu, \nu}$ is the flux operator in the eigenbasis:

$$\hat{j}_{\nu, \mu}(\vec{u}) = \frac{i}{\hbar} \sum_{n, m} (\vec{u} \cdot \vec{r}_{n, m}) \phi_n^{\mu*} \phi_m^\nu \mathcal{H}_{n, m}. \quad (\text{S21})$$

In the expression above, \vec{u} is a unit vector indicating the transport direction, $\vec{r}_{n, m}$ is the vector connecting the positions of site n and m , ϕ_n^ν is the amplitude of the ν eigenstate at site n and $\mathcal{H}_{n, m} = \langle n | \mathcal{H} | m \rangle$ is the coupling between n and m sites. In our 1D system with nearest neighbor interactions, $\vec{u} \cdot \vec{r}_{n, m} = m - n = \pm a$ and $\mathcal{H}_{n, m} = J(\delta_{m, n+1} + \delta_{m, n-1})$. Therefore,

$$\hat{j}_{\nu, \mu} = i \frac{Ja}{\hbar} \sum_n \phi_n^{\mu*} (\phi_{n+1}^\nu - \phi_{n-1}^\nu). \quad (\text{S22})$$

Equation (S20) have been compared with numerical simulations using the QD approach in Figures S4, S5, and S6. It also have been used to study the dependence with N of the diffusion coefficient in various models. Figure S3 shows the diffusion coefficient D of the HHAA model in the three regimes as a function of the dephasing strength for different chain lengths N . We observe for small dephasing a clear dependence of D on the system size. This is due to the fact that when dephasing is small, the excitation reaches the boundaries before diffusion can sets in. Defining the typical time scale for dephasing to affect the dynamics as $\tau_\phi = \frac{\hbar}{\gamma_\phi}$, we can estimate the dephasing strength below which finite size effects are relevant, by comparing τ_ϕ with the time needed to reach ballistically the boundaries for the clean case ($W = 0$). In the ballistic regime ($W < 2J$) the value of decoherence strength below finite size effect starts to be relevant will decrease proportional to $1/N$, while in the diffusive regime ($W = 2J$) with $1/N^2$ (see vertical dashed lines in Figures S3ab). In the localized regime finite size effects are negligible if the system size is larger than the localization length.

B. Analytical expression of the Diffusion coefficient from the coherent dynamics.

The presence of the Haken-Strobl dephasing can be thought as the system being measured by the environment[75, 79]. This measurements occur at random times, where the times between subsequent measurements are distributed

as $p(t) = e^{-t/\tau_\phi}/\tau_\phi$, with $\tau_\phi = \hbar/\gamma_\phi$. In this section, we employ this interpretation of the Haken-Strobl dephasing to obtain analytical expressions for the diffusion coefficient.

When the measurement occurs, the system has a probability distribution of being at the position r , $P_0(r, t, r_0, t_0)$, determined by the coherent Hamiltonian dynamics. The initial position, r_0 at t_0 will only define the center of the probability density, since the system is isotropic. This assumption is valid in the three models treated in this work unless the excitation is close to the boundaries. Consequently, $P_0(r, t, r_0, t_0) = P_0(r - r_0, t - t_0, 0, 0)$. For simplicity we will consider $r_0 = 0$, $t_0 = 0$.

The probability density of measuring the system at site r at time t once the measurement process is included ($\tilde{P}(r, t, 0, 0)$) will be determined by the integral equation:

$$\tilde{P}(r, t, 0, 0) = \underbrace{P_0(r, t, 0, 0) \left(1 - \int_0^t p(t_i) dt_i\right)}_{\text{No Measurement.}} + \underbrace{\int dr_i \int_0^t dt_i p(t_i) \tilde{P}(r, t, r_i, t_i) P_0(r_i, t_i, 0, 0)}_{\text{Measurement at } (t_i, r_i)}, \quad (\text{S23})$$

which recurrently considered the probability of not being measured and of being measured several times.

To directly analyze the second moment of the distribution we multiply by r^2 and integrate over r on both sides:

$$\sigma^2(t) = \sigma_0^2(t) \left(1 - \int_0^t p(t_i) dt_i\right) + \int dr_i \int_0^t dt_i p(t_i) \underbrace{\int dr \tilde{P}(r, t, r_i, t_i) r^2 P_0(r_i, t_i, 0, 0)}_{r_i^2 + \sigma^2(t-t_i)}, \quad (\text{S24})$$

$$\sigma^2(t) = \sigma_0^2(t) \left(1 - \int_0^t p(t_i) dt_i\right) + \int_0^t dt_i p(t_i) \sigma_0^2(t_i) + \int_0^t dt_i p(t_i) \sigma^2(t - t_i), \quad (\text{S25})$$

where we have used the independence of the probabilities from the initial site and time.

It can be shown by Laplace transform in Eq. (S25) (SM. IV B 1), that for well-behaved $p(t)$ and $\sigma_0^2(t)$ (trivially fulfilled in the systems we consider), the dynamics of the variance $\sigma^2(t)$ becomes diffusive at long enough times. Therefore, in the long time limit ($t \rightarrow \infty$) we have:

$$\begin{aligned} \sigma^2(t) &\simeq 2Dt, \\ \left(1 - \int_0^t p(t_i) dt_i\right) &\simeq 0, \\ \int_0^t dt_i p(t_i) t_i &\simeq \tau_\phi, \end{aligned}$$

and,

$$D = \frac{\int_0^\infty dt_i p(t_i) \sigma_0^2(t_i)}{2\tau_\phi}. \quad (\text{S26})$$

Then if $\sigma_0^2(t) = 2D_0 t \forall t$ the measurement process does not affect the diffusion coefficient:

$$D = 2D_0 \frac{\int_0^\infty p(t_i) t_i dt_i}{2\tau_\phi} = D_0. \quad (\text{S27})$$

Another physically relevant case is when the dynamics is initially ballistic up to some time τ_W followed by a diffusive dynamic.

$$\sigma_0^2(t) = \begin{cases} v_0^2 t^2 & \text{if } t < \tau_W \\ 2D_0 t & \text{if } t > \tau_W \end{cases} \quad \text{with } D_0 = \frac{v_0^2 \tau_W}{2} \quad (\text{S28})$$

$$D = \frac{1}{2\tau_\phi} \left(\int_0^{\tau_W} \frac{2D_0}{\tau_W} t^2 p(t) dt + \int_{\tau_W}^\infty 2D_0 t p(t) dt \right) \quad (\text{S29})$$

Considering a Poisson process for the measurements: $p(t) = \frac{e^{-t/\tau_\phi}}{\tau_\phi}$, we have:

$$D(\tau_\phi) = D_0 \left(\frac{2\tau_\phi}{\tau_W} - \left(1 + \frac{2\tau_\phi}{\tau_W}\right) e^{-\tau_W/\tau_\phi} \right), \quad (\text{S30})$$

this expression captures the dependence of D for large and small values of τ , so that $D \approx D_0(1 - \frac{1}{6}(\frac{\tau_W}{\tau_\phi})^2)$ and $D \approx v_0^2 \tau_\phi$ respectively. Note that considering a process $p_\delta(t) = \delta(t - 2\tau_\phi)$, would yield $\tilde{D} = v_0^2 \tau_W = D_0$ for $\tau_\phi > \tau_W/2$ and $\tilde{D} = v_0^2 2\tau_\phi = D_0 2\tau_\phi/\tau_W$ for $\tau_\phi < \tau_W/2$.

1. Analytical solution for the spreading.

In this section we show that Eq. (S25) for $p(t) = e^{-t/\tau_\phi}/\tau_\phi$ generates a diffusive dynamics at long times and find analytical solutions in some paradigmatic cases. Eq. (S25) can be rearranged in the following form:

$$\sigma^2(t) = f(t) + \int_0^t dt_i p(t_i) \sigma^2(t - t_i), \quad (\text{S31})$$

by noting that $(1 - \int_0^t p(t) dt) = e^{-t/\tau_\phi} = \tau_\phi p(t)$ and defining $f(t) = \tau_\phi g(t) + \int_0^t dt_i g(t_i)$ with $g(t) = \sigma_0^2(t)p(t)$.

The usual strategy to solve this type of equation is to use the Laplace's transform on the equation,

$$\sigma_{LT}^2(s) = \mathcal{F}(s) + \sigma_{LT}^2(s) \mathcal{P}(s),$$

where $\sigma_{LT}^2(s)$, $\mathcal{F}(s)$ and $\mathcal{P}(s) = \frac{1}{s\tau_\phi + 1}$ are the Laplace's transform of $\sigma^2(t)$, $f(t)$ and $p(t)$ respectively.

Identifying $\mathcal{G}(s)$ as the Laplace's transform of $g(t)$, we have $\mathcal{F}(s) = \mathcal{G}(s)(\frac{s\tau_\phi + 1}{s})$, and:

$$\sigma_{LT}^2(s) = \frac{\mathcal{F}(s)}{1 - \mathcal{P}(s)} = \mathcal{G}(s) \tau_\phi \frac{(s\tau_\phi + 1)^2}{(s\tau_\phi)^2} = \mathcal{G}(s) \tau_\phi \left[\frac{1}{(s\tau_\phi)^2} + \frac{2}{s\tau_\phi} + 1 \right]. \quad (\text{S32})$$

Since the Laplace transform of $t^n u(t)$, where $u(t)$ is the step function, is $\frac{n!}{s^{n+1}}$ we observe that $\sigma^2(t)$ will be diffusive in the long time limit if $\mathcal{G}(0)$ is finite and non zero, a condition trivially fulfilled in the systems under consideration.

In this case, $D = \frac{\mathcal{G}(0)}{2\tau_\phi} = \frac{\int_0^\infty \sigma_0^2(t)p(t)dt}{2\tau_\phi}$, as we found in Eq. (S26).

The inverse transform of $\sigma_{LT}^2(s)$ can be carried out in several cases (for example $\sigma_0^2(t) = A_\alpha t^\alpha$), however, here we only discuss two paradigmatic cases $\sigma_0^2(t) = 2D_0 t$ and $\sigma_0^2(t) = v_0^2 t^2$. In the first case, the diffusive spreading, we find $\sigma^2(t) = 2D_0 t$, i.e. the dynamic of σ_0^2 is not affected.

In the second case, the ballistic spreading, the solution is

$$\sigma^2(t) = 2\tau_\phi v_0^2 \left(\tau_\phi \left(e^{-\frac{t}{\tau_\phi}} - 1 \right) + t \right), \quad (\text{S33})$$

which for $t \ll \tau_\phi$, $\sigma^2(t) \approx v_0^2 t^2$, maintains its ballistic behavior but becomes diffusive for $t \gg \tau_\phi$, $\sigma^2(t) \approx 2v_0^2 \tau_\phi t = 2Dt$. The same expression is found when the spreading in an ordered tight-binding chain with Haken-Strobl decoherence is addressed with the Lindblad formalism [47, 72].

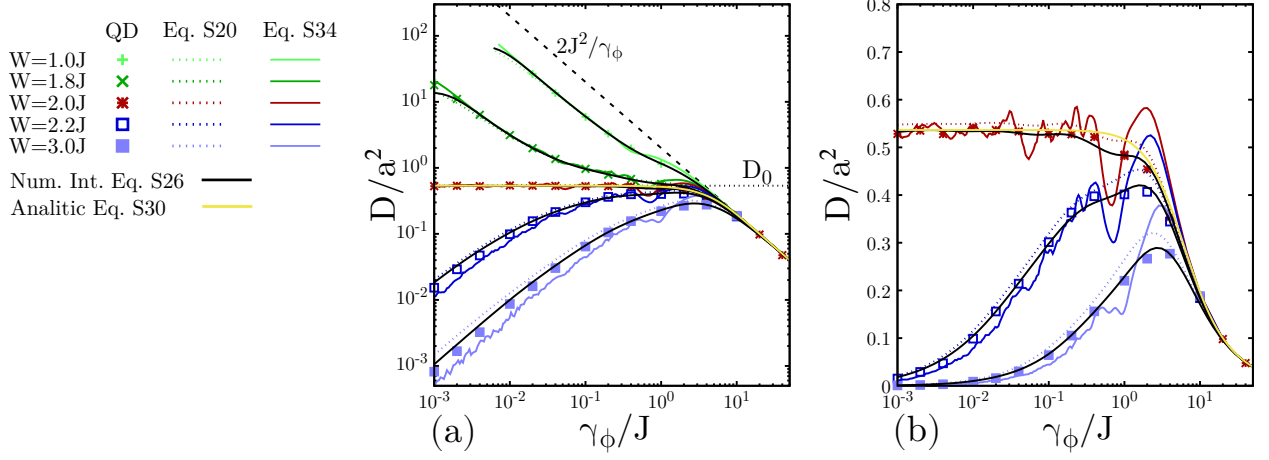
It is important to note that if one considers two Poisson processes, $p_1(t) = e^{-t/\tau_1}/\tau_1$ and $p_2(t) = e^{-t/\tau_2}/\tau_2$, the combined effect will be equivalent to consider only one process with $p(t) = e^{-t/\tau}/\tau$ with $\tau = \frac{\tau_1 \tau_2}{\tau_1 + \tau_2}$, the sum of inverse times scales. This is the standard result in classical systems where one considers a particle that moves with velocity v_0 to the left or right with the same probability after a scattering with either of the two processes. The diffusion coefficient, in this case, is, $D = v_0^2 \tau = v_0^2 \frac{\tau_1 \tau_2}{\tau_1 + \tau_2} = D_1 \frac{1}{1 + \tau_1/\tau_2}$, which for $\tau_2 \gg \tau_1$ generates a linear correction to the diffusion coefficient associated with the process p_1 .

C. Analytical expression of the Diffusion coefficient in the limit of strong and weak dephasing.

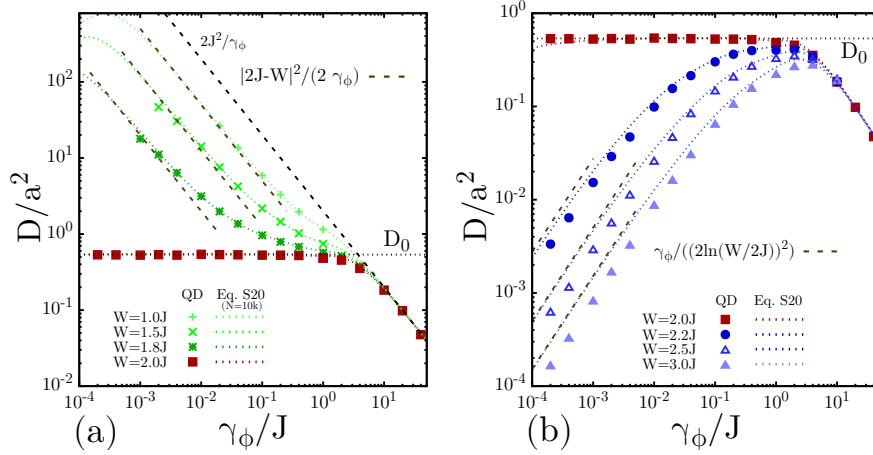
In this section, we use Eq. (S26) and the specific dynamics of $\sigma_0^2(t)$ in the HHAA model (SM III), to obtain the behavior of D in the limit of strong and weak dephasing.

We define the mean free path l from the expectation value of the coherent spreading $l^2 = \int_0^\infty \sigma_0^2(t)p(t)dt$. We compare it with a random walk analysis of the diffusion coefficient [77] which corresponds to a delta process where the system is measured by the environment at equal times $\delta t = 2\hbar/\gamma_\phi$. The diffusion coefficient is directly determined by the coherent spreading at the dephasing time:

$$D = \frac{l^2}{2\delta t} = \frac{\sigma_0^2(t = \frac{2\hbar}{\gamma_\phi})}{2 \frac{2\hbar}{\gamma_\phi}}, \quad (\text{S34})$$



SUPPLEMENTARY FIG. S4. (a,b) Diffusion coefficient vs. the decoherence strength for the HHAA model. Symbols have been obtained from the time evolution, dotted curves from Eq. (S20) [Green-Kubo expresion], solid colored curves from Eq. (S34) [Delta process] and solid black curves from Eq. (S26) [Poisson process]. Also shown : the diffusion coefficient in the strong dephasing regime (dashed lines) and the diffusion coefficient in absence of dephasing at the MIT (D_0) as a horizontal dotted line, see Eq. (S18). The yellow line corresponds to Eq. (S30). (b) is the same as (a) but in linear-log. scale.



SUPPLEMENTARY FIG. S5. Diffusion coefficient vs. the decoherence strength for the HHAA model. Symbols have been obtained from the QD time evolution, dashed curves from the Green-Kubo formula and dashed lines represents the analytical estimations. (a) Extended phase, the analytical results corresponds to Eq. (S36) (dashed-brown lines). (b) Localized phase, the analytical results corresponds to Eq. (S39) (dashed-brown lines). The parameters are $N = 1000$, $Q = (\sqrt{5} - 1)/2$, $J = 1$ and $\hbar = 1$.

this expression, however inaccurate, can be considered a first approximation to the diffusion coefficient.

Figures S4 show the diffusion coefficient obtained from the time evolution (symbols), Eq. (S20) (dotted curves), Eq. (S34) (solid colored-curves) and from numerical integration of Eq. (S26) (solid black-curves). The yellow curve corresponds to Eq. (S30). We observe that using a Poisson process (Eq. (S26)) we obtain results smoother than with a Delta process (Eq. (S34)) (the fluctuations produced by particular interferences are washed-out) and can be obtained at almost the same computational cost.

1. Large dephasing.

For sufficiently large dephasing, $\gamma_\phi \gg \hbar/\tau_W$, the noise interrupts the dynamics before the systems notice if it is in an extended, critical, or localize phase. This is known as the strong Zeno regime. In this case, the measurement happens during the initial ballistic dynamics, where the variance grows as $\sigma_0^2(t) = 2a^2 \frac{J^2}{\hbar^2} t^2$. Therefore, the dynamic

corresponds to a random walk with a mean free path $l^2 = 2a^2 \frac{J^2}{\hbar^2} \delta t^2$ and a mean free time $\delta t = \frac{2\hbar}{\gamma_\phi}$. Thus, the diffusion coefficient is:

$$D = \frac{1}{2} \frac{2a^2 J^2}{(\gamma_\phi/2)^2} \frac{\gamma_\phi}{2\hbar} = \frac{2a^2 J^2}{\hbar \gamma_\phi}. \quad (\text{S35})$$

The same result is obtained with the Poisson process $p(t) = e^{-t/\tau_\phi}/\tau_\phi$. This result is valid for all γ_ϕ for an infinite clean chain ($W = 0$) [72], since in that case $\tau_W \rightarrow \infty$.

2. Extended phase ($W < 2J$).

For sufficiently small dephasing strength (depending on how close we are to the MIT), the system enters the long-time ballistic regime where $\sigma_0^2(t) = \frac{a^2|2J-W|^2}{2\hbar^2} t^2$ from which we have:

$$D = \frac{a^2|2J-W|^2}{2\hbar \gamma_\phi}. \quad (\text{S36})$$

Note that as we approach the MIT our estimate is valid for a smaller and smaller dephasing strength since the system enters the ballistic regime at larger times. Using the Poisson process $p(t)$ and Eq. (S26) we obtain the same results. In Fig. S5a we compare the diffusion coefficient obtained from the numerical simulations (symbols) with the analytical approximation Eq. (S36).

3. MIT ($W = 2J$).

At the critical point, for $t > \tau_W$ the dynamic is diffusive and the variance is linearly dependent on the measurement time $\sigma_0^2(\delta t) = 2D_0\delta t$. Given that we have $l^2 = 2D_0\delta t$, provided that $\gamma_\phi < 2\hbar/\tau_W$, and $D = l^2/(2\delta t)$ we obtain:

$$D = \frac{2D_0\delta t}{2\delta t} = D_0, \quad (\text{S37})$$

i.e. a diffusion coefficient independent of the dephasing.

This was shown to be exact for an always diffusive dynamic in SM IV B. On the other hand when we consider a ballistic dynamics for short times and a Poisson measurement process some corrections appear.

4. Localized phase ($W > 2J$).

For sufficiently small dephasing strength (depending on how close we are to the MIT), the system gets localized with a localization length $\xi = l/\sqrt{2}$ before dephasing sets in. So, considering $\sigma_0^2 = l^2$ in Eq. S26:

$$\sigma^2(t) = \frac{l^2}{\tau_\phi} t = l^2 \frac{\gamma_\phi}{\hbar} t = 2\xi^2 \frac{\gamma_\phi}{\hbar} t. \quad (\text{S38})$$

This limit is also found in Ref. [48] from Eq. S20. Since in the HHAA model $2\xi^2 = 2a^2(2\ln(W/2J))^{-2}$, the diffusion coefficient is:

$$D = \frac{\xi^2 \gamma_\phi}{\hbar} = \frac{a^2 \gamma_\phi}{(2\ln(W/2J))^2 \hbar}. \quad (\text{S39})$$

The analytical result is shown in Fig. S5b compared with the numerical results. We observe a small discrepancy with the above formula, rooted in the fact that the numerically found l^2 is slightly smaller than the theoretical one.

Notice that, in contrast with the other regimes, the delta and Poisson process do not yield the same expression (the use of a delta process would underestimates the diffusion coefficient by a factor of two).

V. HHAA MODEL WITH DIFFERENT VALUES OF q .

The diffusion coefficient derived for the critical point in absence of dephasing (Eq. (S18)) shows a dependence on q . In order to check the validity of our analytical prediction and the generality of the dephasing-independent regime we analyzed other irrational values of q , beyond the golden mean value used in the main text.

Particularly we study the dynamics of the system using fractions of the golden ratio as irrational numbers $q = q_g/m$, where m is an integer power of two. The continued fractions of the irrationals used are presented in Table I. Trials with irrational numbers of the form $[0, \{m\}]$ yielded similar results.

The spreading in time of the wave packet in absence and presence of dephasing together with our analytical estimations for the diffusion coefficient is shown in Fig. S6a,b. As one can see, the initial ballistic spreading (Eq. (S13)) lasts until a time τ_W (Eq. (S17), indicated as vertical lines in Fig. S6a,b). After that time the dynamics is diffusive with a diffusion coefficient given by Eq. (S18). We notice, see panel (a), the presence of oscillations in the second moment which increase as q decreases. These oscillations are partly erased in presence of dephasing at long times as shown in Fig. S6b for $\gamma_\phi = 0.02$.

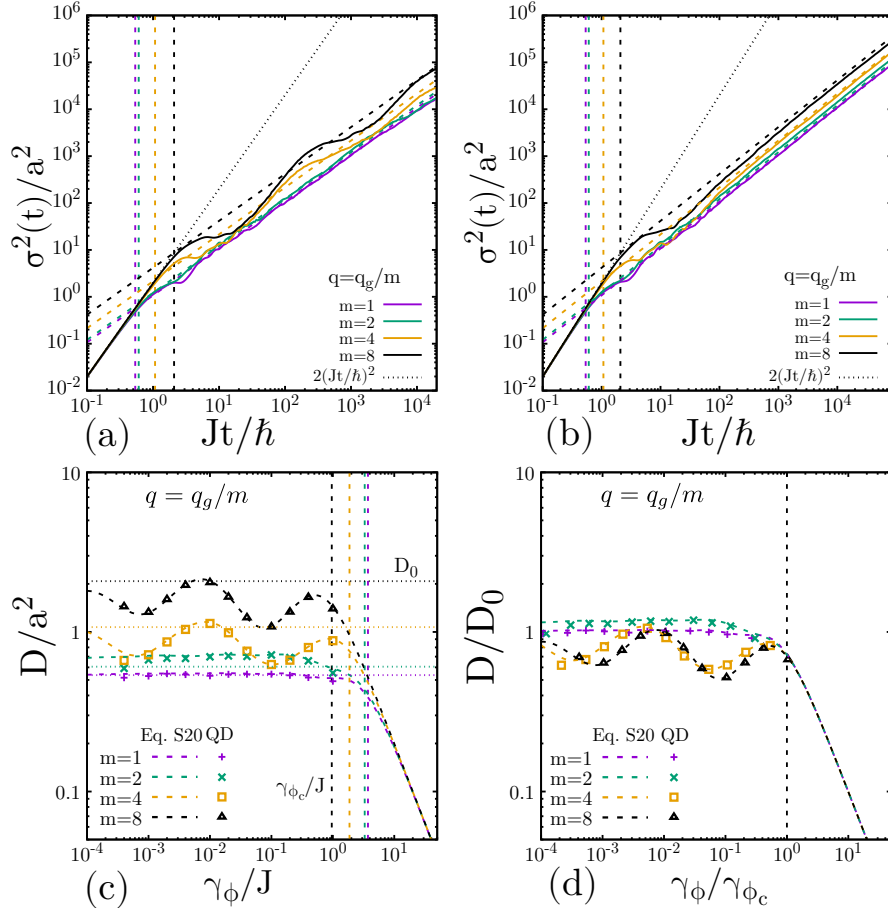
Fig. S6c shows the fitted values of D (symbols) together with the D values obtained from Eq. (S20) (dashed curves) as a function of γ_ϕ for different q at the MIT. As vertical dashed lines, we plot $\gamma_\phi^c = \frac{2\hbar}{\tau_W}$ which coincide with the beginning of the strong dephasing regime, where the diffusion coefficient decreases with dephasing. Notice that for large values of m the diffusion coefficient D presents wide oscillations as a function of γ_ϕ , probably due to a weaker irrationality of the q value. More investigations should be done in the future to understand the origin of these interesting oscillations. In Fig. S6d we plot the diffusion coefficient re-scaled by the theoretical value in absence of dephasing (Eq. (S18)) and γ_ϕ re-scaled by the elastic scattering rate $\gamma_\phi^c = \frac{2\hbar}{\tau_W}$. Fig. S6d confirm the validity of our analytical expressions of D and τ_W as a function of q .

TABLE I. Continued fraction of the irrational used in this section $q = q_g/m$. The numbers between brackets are infinitely repeated in the fraction.

Continued Fraction	
$\frac{\sqrt{5}-1}{2} = [0, \{1\}]$	$= \frac{1}{1 + \frac{1}{1 + \dots}}$
$\frac{1}{2} \frac{\sqrt{5}-1}{2} = [0, 3, \{4\}]$	$= \frac{1}{3 + \frac{1}{4 + \frac{1}{4 + \dots}}}$
$\frac{1}{4} \frac{\sqrt{5}-1}{2} = [0, 6, \{2, 8\}]$	$= \frac{1}{6 + \frac{1}{2 + \frac{1}{8 + \frac{1}{2 + \dots}}}}$
$\frac{1}{8} \frac{\sqrt{5}-1}{2} = [0, 12, \{1, 16\}]$	$= \frac{1}{12 + \frac{1}{1 + \frac{1}{16 + \frac{1}{1 + \dots}}}}$

VI. STUDY OF DIFFERENT PARADIGMATIC MODELS OF TRANSPORT.

In this section we test the validity of Eq. (S16) and Eq. (S26), using two models that present a coherent diffusion regime and/or criticality: the Fibonacci chain, and the Power-Banded Random Matrices (PBRM) model.



SUPPLEMENTARY FIG. S6. Upper panels: Time evolution of the spreading of an excitation in a HHAA chain with $q = q_g/m$ at criticality. The vertical-dashed lines show τ_W (Eq. (S17)), the crosswise dashed lines correspond to $\sigma^2(t) = 2D_0t$ (Eq. (S18)), while the dotted line shows the initial ballistic evolution (Eq. (S13)). (a) $\gamma_\phi = 0$, (b) $\gamma_\phi = 0.02$. Bottom panels: (c): Diffusion coefficient as a function of the dephasing strength γ_ϕ . D is calculated from the QD dynamics (symbols) and from Eq. (S20) (dashed lines). The horizontal-dotted shows D_0 (Eq. (S18)) and the vertical-dashed lines $\gamma_\phi^c = \frac{2\hbar}{\tau_W}$. (d): The diffusion coefficient and dephasing strength are re-scaled by D_0 and γ_ϕ^c respectively. Parameters are $N = 10000$, $W = 2J$.

A. The Fibonacci chain.

The Fibonacci model is described by the Hamiltonian:

$$\mathcal{H} = \sum_n J(|n\rangle\langle n+1| + |n+1\rangle\langle n|) + \varepsilon_n |n\rangle\langle n|, \quad (\text{S40})$$

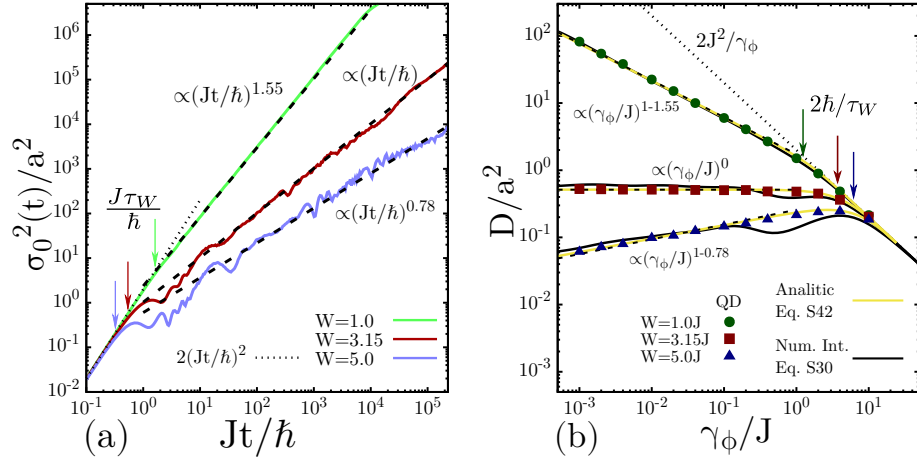
where the on-site potential is determined by $\varepsilon_n = W([\!(n+1)q_g^2] - [nq_g^2])$, here $[x]$ represents the integer part of x and $q_g = \frac{\sqrt{5}-1}{2}$ is the golden ratio. In this potential, ε_n corresponds to the n -th element of the Fibonacci word sequence, that can also be obtained by repeated concatenation: 0, 0W, 0W0, 0W00W, 0W00W0W0, etc.

The dynamics in the Fibonacci chain were studied in absence and presence of dephasing [49, 94, 133]. In absence of dephasing it is known that the second moment grows, after the initial quadratic spreading, as a power law $\sigma_0^2(t) \propto t^\alpha$ with an exponent that depends on the strength of the on-site potential. It grows subdiffusively ($\alpha < 1$) for $W > 3.15J$, diffusively ($\alpha = 1$) for $W = 3.15J$ and superdiffusively ($\alpha > 1$) for $W < 3.15J$. These dynamics are shown in Fig. S7a.

This spreading can be written analytically in the approximated and simplified form:

$$\sigma_0^2(t) = \begin{cases} v_0^2 t^2 & \text{if } t < \tau_W \\ 2At^\alpha & \text{if } t > \tau_W \end{cases} \quad \text{with } A = \frac{v_0^2 \tau_W^{2-\alpha}}{2}. \quad (\text{S41})$$

From this expression and using Eq. (S26) with a Poisson process we obtain an analytical expression for the diffusion



SUPPLEMENTARY FIG. S7. (a) Time evolution of the spreading in absence of dephasing for $W = \{1, 3.15, 5\}$ in the Fibonacci chain. The dotted-black lines show the initial ballistic spreading (Eq. (S13)), the vertical arrows τ_W (Eq. (S16)), and the dashed-black lines show the power law behavior after τ_W . (b) Diffusion coefficient as a function of the dephasing strength. The symbols are fitted directly from the QD dynamic in presence of dephasing, the solid-black curves show Eq. (S26) numerically integrated using a Poisson process, and as solid-yellow curves the analytical expression Eq. (S42) is plotted. The vertical arrows correspond to $2\hbar/\tau_W$, where the strong dephasing regime indicated by a dotted-black line starts. The dashed-black lines indicate the power dependence for small γ_ϕ . The simulations were done in a chain of length $N = 10^4$.

coefficient in presence of dephasing:

$$D = \frac{v_0^2 \left(\tau_W^3 E_{-\alpha} \left(\frac{\tau_W}{\tau_\phi} \right) + \alpha \tau_\phi \tau_W^2 \Gamma(\alpha) \left(\tau_\phi^\alpha \tau_W^{-\alpha} - \left(\frac{\tau_W}{\tau_\phi} \right)^{-\alpha} \right) + 2\tau_\phi^3 - \tau_\phi e^{-\frac{\tau_W}{\tau_\phi}} \left(2\tau_\phi^2 + 2\tau_\phi \tau_W + \tau_W^2 \right) \right)}{2\tau_\phi^2}, \quad (\text{S42})$$

where $\Gamma(\alpha)$ is the Euler Gamma function, and $E_{-\alpha} \left(\frac{\tau_W}{\tau_\phi} \right) = \int_1^\infty e^{-\left(\frac{\tau_W}{\tau_\phi}\right)t} t^\alpha dt$.

The vertical lines in Fig. S7a, represent τ_W , calculated from the analytical equations Eq. (S15) and Eq. (S16) yielding $1/\tau_W = q_g W/\hbar$. After this time, the initial ballistic dynamic stops and the algebraic dynamic starts. Particularly, for $W = 3.15J$, when the subsequent dynamic is diffusive, we obtain $D_0 = \frac{v^2 \tau_W}{2}$. This analytical prediction is shown as a black-dashed line on top of the red curve.

Once dephasing is added, the dynamics becomes diffusive for all values of W . The diffusion coefficient as a function of the dephasing strength was computed numerically through a quantum drift dynamics for different values of W . These results are shown as symbols in Fig. S7b. They are compared with the numerical integration of Eq. (S26) using a Poisson process (black curves) and the analytical expression (Eq. (S7), yellow curves). We conclude that the diffusion coefficient depends only on the coherent dynamics and the noise strength.

From equations (S34) and (S42), it is clear that the dependence of $\sigma_0^2(t)$ determines the behavior of $D(\gamma_\phi)$. Particularly, if $\sigma_0^2(t) \propto t^\alpha$ then $D(\gamma_\phi) \propto (\gamma_\phi)^{(1-\alpha)}$ for $\gamma_\phi \ll 2\hbar/\tau_W$. This dependence is pointed out in Fig. S7b with dashed-black lines on top of the data. These results are consistent with recent findings reported in Ref. [49].

B. The PBRM model.

The power-law banded random matrix (PBRM) model describes one-dimensional (1D) tight-binding chains of length N with long-range random hoppings. This model is represented by $N \times N$ real symmetric random matrices whose elements are statistically independent random variables characterized by a normal distribution with zero mean and variance given by,

$$\langle |\mathcal{H}_{ii}|^2 \rangle = J^2 \text{ and } \langle |\mathcal{H}_{ij}|^2 \rangle = J^2 \frac{1}{2} \frac{1}{1 + (|i-j|/b)^{2\mu}} \text{ with } i \neq j. \quad (\text{S43})$$

The PBRM model, Eq. (S43), depends on two control parameters: μ and b , while J is an energy scale that can be considered equal to 1 for all practical purposes. For $\mu > 1$ ($\mu < 1$) the PBRM model is in the insulating (metallic)

phase, so its eigenstates are localized (delocalized). At the MIT, which occurs for all values of b at $\mu = 1$, the eigenfunctions are known to be multi-fractal.

The statistical properties of the eigenfunctions and eigenvalues of this model have been widely studied[34, 95, 96, 131, 132]. Here we study the spreading dynamics of an initially localized excitation at the middle of the chain in absence and presence of a decoherent environment.

As in the previous systems, the initial spreading of the local excitation is ballistic, where the second moment is given by $\sigma_0^2 = v_0^2 t^2$. Generalizing Eq. (S13) to account for the randomness of the Hamiltonian, we found that the velocity v_0 is:

$$v_0^2 = 2 \sum_{n=1}^{N/2} \langle \mathcal{H}_{n,0}^2 \rangle n^2 = \sum_{n=1}^{N/2} \frac{J^2}{1 + (n/b)^{2\mu}} n^2, \quad (\text{S44})$$

where we summed over the sites to the right and left (factor 2) of the initial site (denoted as 0). This initial velocity (Eq. (S44)) diverges for $\mu < 3/2$ at large N as $N^{3-2\mu}$. For large N , $b \ll 1$, and $\mu < 3/2$, the sum can be approximated by an integral, yielding $v_0^2 \approx J^2 b^{2\mu} \frac{N^{3-2\mu}}{(3-2\mu)2^{3-2\mu}}$.

This initial ballistic spreading lasts up to $t = \tau_W$, which should be addressed numerically since Eq. (S15) is only valid for NN chains and a similar analysis with this model does not yield a simple expression. However, on a first approximation if we use Eq. (S15), with uncorrelated and Gaussian distributed site energies with $\langle |\mathcal{H}_{ii}|^2 \rangle = J^2$, we obtain $\tau_W = 1$.

For $t > \tau_W$, we find numerically that for $0.5 < \mu < 1.5$ the second moment of the excitation spreads diffusively (see Fig. S8a for $\mu = 1$). Note that the parameter b modifies the initial velocity and the diffusion coefficient. Consequently, we choose a small $b = 0.01$ to reduce both the magnitude of the initial spread and the diffusion coefficient, generating a slower dynamic and having a larger window for diffusive dynamics before the system reaches saturation (at fixed N). In the diffusive regime, we find $\sigma_0^2 \approx v_0^2 (\sqrt{2} \tau_W) t$. The factor $\sqrt{2}$ is introduced based on the numerical results to correct the discrepancy in τ_W due to the long-range hopping.

It's important to note that, although the system is localized for $1.0 < \mu < 1.5$, its eigenfunctions have power-law tails with exponent 2μ , therefore its second moment diverges $N \rightarrow \infty$. The presence of these fat tails allows an unbounded growth in time of the second moment in the limit of $N \rightarrow \infty$. For $\mu < 1.5$ the saturation value of the second moment $\sigma_{0,SV}^2$ is $\sigma_{0,SV}^2 = \frac{N^2}{12} f(b, \mu)$, where $f(b, \mu) \leq 1$.

Thus, for $\mu < 1.5$ and assuming a spreading form $\sigma_0^2(t > \tau_W) = v_0^2 \tau_W^2 + \sqrt{2} v_0^2 \tau_W (t - \tau_W)$, we can calculate the time t_s where the spreading reaches its saturation value by imposing $\sigma_{0,SV}^2 = \sigma_0^2(t_s)$ obtaining:

$$t_s = \frac{\sigma_{0,SV}^2}{\sqrt{2} v_0^2 \tau_W} + \tau_W \frac{(\sqrt{2} - 1)}{\sqrt{2}} \propto N^{2\mu-1}. \quad (\text{S45})$$

Our analytical estimate of t_s agrees with the numerical finding (see, Fig. S8a for $\mu = 1$). Eq. (S45) implies that as N increases, for $\mu < 1/2$ the saturation value will be reached at shorter times and eventually the dynamics will be always ballistic (t_s becomes smaller than τ_W). On the opposite case, for $1/2 < \mu < 3/2$, t_s increases with N and we have a diffusive spreading until saturation.

As in the previous models, the presence of a coherent quantum diffusion (for $1/2 < \mu < 3/2$), generates an almost decoherence-independent diffusive regime. Indeed, for $2\hbar/t_s \lesssim \gamma_\phi \lesssim 2\hbar/\tau_W$, D is almost constant, as most of the *environmental measurements* fall in the diffusive regime (after τ_W and before the saturation time t_s). When $\gamma_\phi \ll 2\hbar/t_s$ the noise enters in the dynamics after saturation, generating finite size effects. From Eq. (S45) we can see that for $1/2 < \mu < 3/2$, t_s increases with N , and finite size effects start at smaller values of the decoherence strength, see Fig. S8b. For $\gamma_\phi > 2\hbar/\tau_W$, decoherence affects the dynamics mainly during the initial ballistic spreading, leading to a decrease of the diffusion coefficient proportional to v_0^2 .

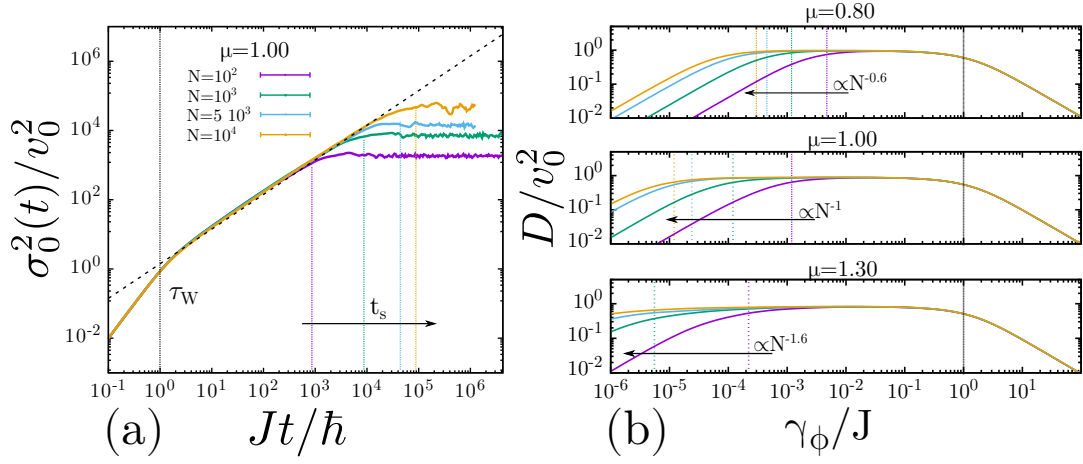
For $\mu < 1/2$, the velocity of the initial ballistic spreading, see Eq. (S44), increases with N faster than that saturation value. Therefore, t_s decreases with N , becoming smaller than τ_W and leaving no place for a diffusive dynamic. Hence, no decoherence-independent region can be found for the diffusion coefficient.

For $\mu > 3/2$, t_s converges to a constant value as N increases. Thus, for $\gamma_\phi < 2\hbar/t_s$ the diffusion coefficient will be linearly dependent on γ_ϕ and we can not have a dephasing independent regime. This situation is similar to the localized case of the Harper-Hofstadter-Aubry-André.

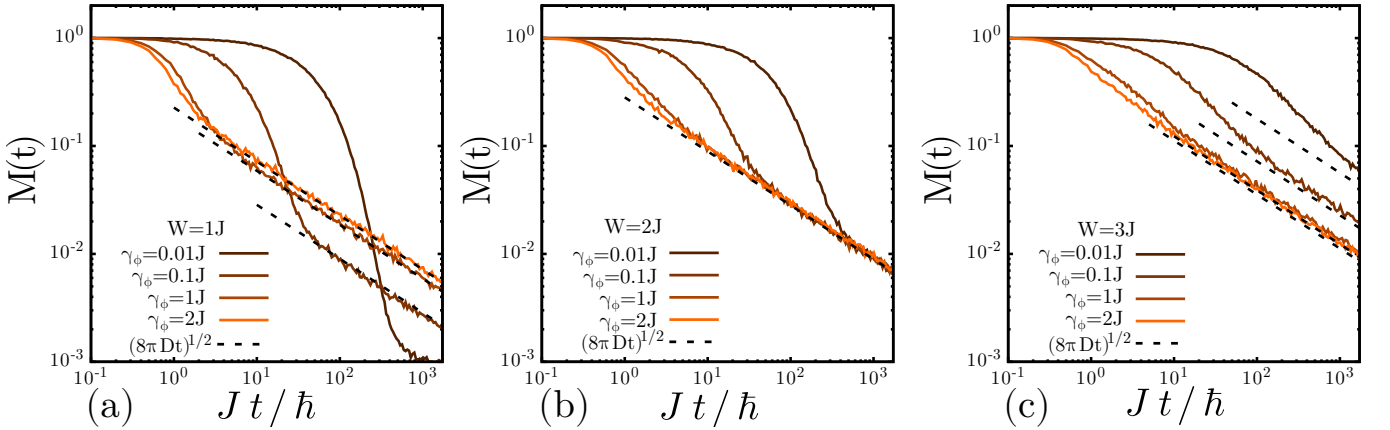
VII. PURITY.

The purity, defined as,

$$M(t) = \text{Tr}[\rho(t)\rho(t)], \quad (\text{S46})$$



SUPPLEMENTARY FIG. S8. (a) Time evolution of the spreading of an initially localized excitation in absence of dephasing in the PBRM model for $\mu = 1$, $b = 0.01$, and $N = \{100, 1000, 5000, 10000\}$. The vertical lines denote τ_W (black) and t_s (colored), while the crosswise dashed line represents the theoretical diffusive spreading $\sigma_0^2(t)/v_0^2 \approx \sqrt{2}t$. (b) From top to bottom the figures shows the diffusion coefficient obtained through Eq. (S20) for $\mu = \{0.80, 1.00, 1.30\}$. The vertical dashed-black line marks the characteristic dephasing where the dynamics start to be dominated by noise and the initial ballistic dynamics (strong Zeno regime). The colored dashed vertical lines show the values of $\gamma_\phi = 2\hbar/t_s$ below which finite size effect starts to be relevant, the dependence with N of the values is indicated in each plot.



SUPPLEMENTARY FIG. S9. Time evolution of the purity (Loschmidt echo) $M(t)$ with different dephasing strength in a HHAA chain with $N = 1000$. (a) $W = J$, extended phase. (b) $W = 2J$, MIT. (c) $W = 3J$, localized phase. The dashed-black lines are theoretical predictions ($M(t) \propto \frac{1}{\sqrt{Dt}}$) where D was obtained from Eq. (S20) for Fig. (a) and (c) and from Eq. (S18) for (b).

where $\rho(t) = e^{\mathcal{L}t} \rho_0$ is the evolved density matrix, is a measure of the coherence's level of $\rho(t)$. $M(t) = 1$ implies that $\rho(t)$ is a pure state (fully coherent), while $M(t) < 1$ indicates a mixed state (incoherent superposition).

In the following we show that the purity can be calculated using the quantum drift (QD) simulation by generating a Loschmidt echo in the dynamics.

The superoperator \mathcal{L} is defined by,

$$\mathcal{L}[\rho] = -\frac{i}{\hbar} [\mathcal{H}\rho - \rho\mathcal{H}] + \mathcal{L}_\phi[\rho] = \mathcal{L}_0 + \mathcal{L}_\phi, \quad (\text{S47})$$

where \mathcal{H} is the Hamiltonian and \mathcal{L}_ϕ the HS dephasing. We can see that $\mathcal{L}^\dagger = \mathcal{L}_0^\dagger + \mathcal{L}_\phi^\dagger = -\mathcal{L}_0 + \mathcal{L}_\phi$, and since the density matrix is a Hermitian operator, we have, $\rho(t) = \rho^\dagger(t) \implies e^{\mathcal{L}t} \rho_0 = \rho_0 e^{\mathcal{L}^\dagger t}$. Using these properties we rewrite the definition of the purity in the following form,

$$M(t) = \text{Tr}[\rho(t)\rho(t)] = \text{Tr}[e^{\mathcal{L}t} \rho_0 e^{\mathcal{L}t} \rho_0] \quad (\text{S48})$$

$$= \text{Tr}[\rho_0 e^{\mathcal{L}^\dagger t} e^{\mathcal{L}t} \rho_0] \equiv \text{Tr}[\rho_0 \rho_{LE}(2t)], \quad (\text{S49})$$

where it is clear that the purity is a comparison between the initial density matrix and the density matrix $\rho_{LE}(2t)$ which is the result of two evolutions. In details, there is an initial forward evolution $\rho(t) = e^{(\mathcal{L}_0 + \mathcal{L}_\phi)t} \rho_0$ and a second evolution with the sign of the Hamiltonian inverted (backward evolution) $\rho_{LE}(2t) = e^{(-\mathcal{L}_0 + \mathcal{L}_\phi)t} \rho(t)$, i.e. the purity corresponds to the echo observed on ρ_0 after reverting the time. If the initial state is a pure state $\rho_0 = |0\rangle\langle 0|$, we can directly obtain the purity numerically by a stochastic simulation of the forward and backward evolution and by looking at the probability of returning to the initial state (in our case, the initial site).

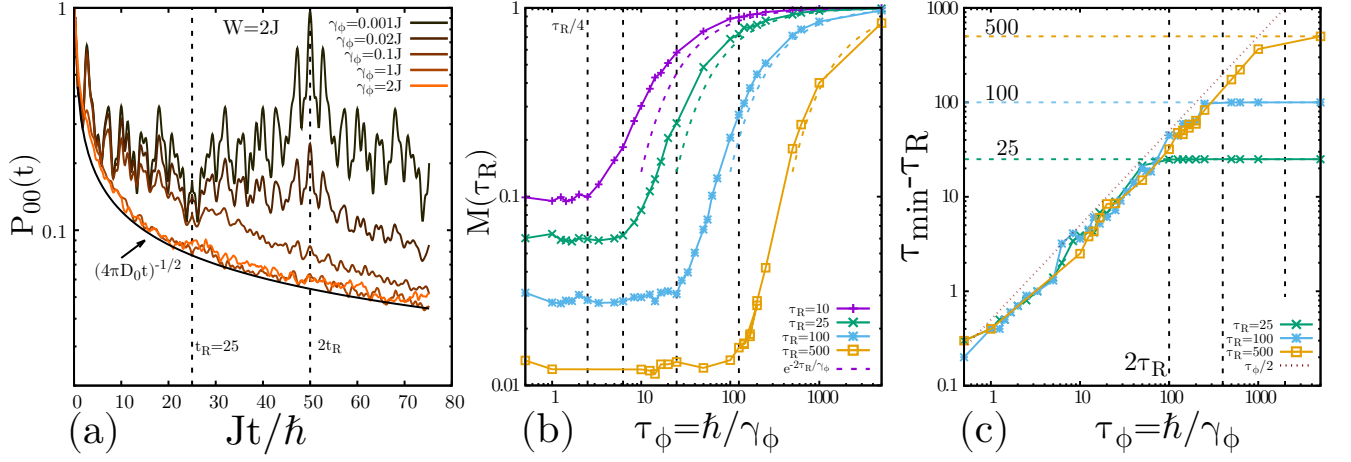
We studied the purity as a function of time in the extended, critical, and localized regimes in the HHAA model changing the decoherence strength. These results are shown in Figures S9. We observe that for short times the decay of the purity is exponential and only depends on the decoherence strength and the initial state in all regimes. After $t \approx 4\hbar/\gamma_\phi$ (numerically estimated), the decay of the purity becomes a power law, $M(t) \propto \frac{1}{\sqrt{D(\gamma_\phi, W)t}}$, where $D(\gamma_\phi, W)$ is the diffusion coefficient of the forward dynamics (dashed curves in Fig. S9). From the results of the previous sections (for $\gamma_\phi < \gamma_\phi^c$) we infer that the rate of decay of the purity in this power-law regime decreases with γ_ϕ in the extended regime, increases in the localized regime, and remains constant at the critical point. This can be interpreted by considering that the localized states are more protected from decoherence, as decoherence affects fewer sites. In this case, as we increase the decoherence strength the decay of the purity is stronger in both the short and long time regimes as a consequence of the delocalization of the wave function. Secondly, in the extended regime, while a stronger decoherence causes a faster decay in the purity at short times, at large times, where the forward dynamics determine the decay rate, it becomes slower for stronger decoherence. This counter-intuitive result is understood as a consequence of the ballistic growth of the wave packet, which in the large time makes it more sensitive to fluctuations.

To clarify the behavior of $M(t)$ at the MIT, we show in Fig. S10a the evolution of P_{00} (probability of being at the initial site), where the Hamiltonian is reverted at time τ_R . At the LE-time, $t = 2\tau_R$, one has $P_{00}(2\tau_R) = M(\tau_R)$. For $\gamma_\phi \ll \hbar/\tau_R$, we observe that the $P_{00}(t)$ returns to the initial site and an echo is formed. Note that in absence of dephasing the return is complete and the purity is 1. However, if $\tau_R \gg 4\hbar/\gamma_\phi$, $P_{00}(2\tau_R)$ is only determined by the forward diffusive dynamic without a significative echo formation. There are no coherences left to reconstruct the initial dynamic and therefore no echo (peak) is observed, i.e. the $P_{00}(t)$ keeps decaying even with the Hamiltonian reverted. This means that the memory of the initial state is completely lost. Thus, the density matrix is the incoherent superposition of all possible histories. In this sense, after $4\hbar/\gamma_\phi$ the diffusive spreading observed at the MIT differs from the coherent quantum diffusion in the fact that the dynamics it is no longer reversible.

This purity behavior at the MIT is summarized Fig. S10b, where the value of the echo (purity) for different τ_R are shown as a function of $\tau_\phi = \hbar/\gamma_\phi$, as one can see, we observed a constant plateau up to $\tau_\phi \approx \tau_R/4$ indicated by vertical dashed-black lines. After that, we have an exponential growth up to the value 1.

Similar results are found by looking at the width of the returned packet. This is shown in Fig. S10c, where the time at which the second moment reaches its minimum (counted from the reversal time τ_R), is plotted as a function of τ_ϕ . After the change in the Hamiltonian sign the wave function starts to shrink, however, this shrinking lasts until the echo time ($2\tau_R$) only if $\tau_\phi > 2\tau_R$. This is shown in Fig. S10c as a plateau. When $\tau_\phi < 2\tau_R$, the width of the wave packet reaches its minimum at approximately $t \approx \tau_\phi/2$ and starts to broaden again. It is interesting to note that for $2\hbar/\tau_R < \gamma_\phi < 4\hbar/\tau_R$, the wave function is widening again but we observe an echo in the polarization.

We observed that the dependence of the diffusion coefficient with the dephasing strength is inherited by purity (LE) dynamics, as for long times it decays with a power law depending only on D . As a consequence, the purity decay at the critical point enters an almost dephasing-independent decay. However, this regime differs substantially from the chaos-induced LE perturbation independent decay proposed by Jalabert & Pastawski[88], as we might have hinted from Ref. [57]. Indeed, in our case the correlation length of the noise fluctuations is smaller than the mean free path, which does not satisfy the conditions needed for a perturbation-independent decay of the LE. For our local noise, the Feynman history that has suffered a collision with the noisy potential loses the memory of where it comes from, thus it is irreversible as in the Büttiker's dephasing voltage probe. In that sense, the environment-independent decay of the LE/purity, should not be interpreted in the perturbation-independent decoherence context, but rather as a strong irreversibility.



SUPPLEMENTARY FIG. S10. (a) Probability to find the particle in the initial site $P_{00}(t)$ for a HHAA chain with $W = 2J$. Up to time τ_R ($\tau_R = 25$, vertical dashed line) the system evolves with \mathcal{L} , hereon the sign of the Hamiltonian is inverted (the system evolves with \mathcal{L}^\dagger). The value of $P_{00}(t)$ at $2\tau_R$ (echo, second vertical dashed line) corresponds to the purity of the system at the time τ_R ($M(\tau_R)$). (b) Purity (echo) at a fixed time $\tau_R = \{10, 25, 100, 500\}$ as a function of the dephasing time $\tau_\phi = \hbar/\gamma_\phi$ in a HHAA chain with $W = 2J$. The vertical black dashed lines mark $\tau_R/4$, while the colored dashed lines show the analytical behavior for $\tau_\phi \ll \tau_R$. (c) Time at which the variance of the wave packet reaches its minimum after a Hamiltonian inversion at τ_R in a HHAA chain with $W = 2J$. Vertical black dashed lines represent $2\tau_R$ while the horizontal colored-dashed lines stand for τ_R .